

Correction to Luminosity Measurement for the Pixel Luminosity Telescope at CMS

A Thesis Presented for the

Master of Science

Degree

The University of Tennessee, Knoxville

Krishna Thapa

December 2016

© by Krishna Thapa, 2016

All Rights Reserved.

To my parents

Acknowledgements

I would like to thank my advisor, Dr. Stefan Spanier, for allowing me to participate in this part of the CMS collaboration. I learned a great deal from you, not only about physics but also on how to go about solving problems.

Thanks to Mark Foerster for helping me get acquainted with the BRILDAQ infrastructure. Thanks to Grant Riley, who helped me tremendously answering my questions about detectors and ROOT. Thanks to Keith Rose for helping me set up codes, and also for going through the rough draft of my thesis. Thanks to Joe for going through the analysis code and calculating corrections with new data.

Thanks to Paul Lujan for helping me make the dip processor robust by providing helpful feedbacks, and also for providing me the references for the trigger system. Thanks to Anne Dabrowski, David Stickland, Chris Palmer, Arkady Lokhovitskiy and others at the BRIL team for helping me contribute to the development of analytical tools.

हरियो डाँडा माथि हलो बोक्ने साथि हो हो माले होहो...

Abstract

The search for and detailed study of new particles and forces with the Compact Muon Solenoid (CMS) detector at the Large Hadron Collider (LHC) of CERN is fundamentally dependent on the precise measurement of the rate at which proton-proton collisions produce any particles, the so-called luminosity. Therefore, a new detector, the Pixel Luminosity Telescope (PLT), dedicated to measure the luminosity at high precision was added to the CMS experiment in 2015. It measures the inclusive charged particle production from each collision of proton bunches in the LHC. Additional charged particles which are observed by the instrument but produced from sources other than collisions are characterized by measurements of particle trajectories and subtracted from the luminosity. Methods were developed to calculate the corrections to the luminosity measurement of the PLT.

Table of Contents

| | | |
|----------|--|-----------|
| 1 | Introduction | 1 |
| 2 | Physics Background | 3 |
| 2.1 | Standard Model of Particle Physics | 3 |
| 2.2 | Luminosity | 5 |
| 2.3 | Luminosity Calibration | 10 |
| 2.4 | Luminosity Measurement | 12 |
| 3 | Experimental Setup | 15 |
| 3.1 | Large Hadron Collider | 15 |
| 3.1.1 | Filling Scheme | 17 |
| 3.1.2 | LHC Operations in 2015 and 2016 | 17 |
| 3.2 | CMS | 19 |
| 3.3 | Silicon Pixel Detectors | 24 |
| 3.4 | Pixel Luminosity Telescope | 25 |
| 3.4.1 | Triple coincidence measurement | 30 |
| 3.4.2 | Zero Counting Algorithm | 31 |
| 3.4.3 | Van der Meer Scan Calibration | 32 |
| 4 | Operations of PLT | 35 |
| 4.1 | Introduction | 35 |
| 4.2 | Machine condition monitoring | 35 |

| | | |
|-------------------------------------|---|-----------|
| 4.2.1 | Hit Display | 35 |
| 4.2.2 | Coincidences count | 36 |
| 4.3 | Alarm Mechanism | 37 |
| 4.4 | Elastic Search - Data warehousing | 38 |
| 4.5 | Data Validation | 38 |
| 5 | Event Reconstruction | 40 |
| 5.1 | Telescope Alignment | 40 |
| 5.2 | Fast-or triple fold coincidences | 41 |
| 5.3 | Slink Tracks | 45 |
| 6 | Determination of the Luminosity Correction | 49 |
| 6.1 | Introduction | 49 |
| 6.2 | Firmware Issue | 51 |
| 6.3 | Accidental Correction | 53 |
| 6.3.1 | Track Parameters | 53 |
| 6.3.2 | 5 Sigma Cut Procedure | 55 |
| 6.3.3 | Maximum Likelihood Fits | 56 |
| 6.3.4 | Fit Validation | 59 |
| 6.4 | Results | 59 |
| 6.4.1 | Toy Monte Carlo Simulation | 60 |
| 6.5 | Conclusion | 63 |
| Bibliography | | 64 |
| Appendix | | 68 |
| A Pixel Luminosity Telescope | | 69 |
| A.1 | PLT Channel Map | 69 |
| A.2 | Zero - Counting Algorithm | 69 |

List of Tables

| | | |
|-----|--|----|
| 2.1 | Relative strengths of the four fundamental forces in terms of coupling constants. The coupling constant for each force is dimensionless. . . . | 4 |
| 2.2 | LHC beam parameters relevant for the peak luminosity Bailey and Collier (2004) | 8 |
| 5.1 | Time units | 42 |
| 6.1 | Variation in the measured accidental rate with different sets of cuts in track parameters. | 56 |
| A.1 | PLT Channel Map -Z | 69 |
| A.2 | PLT Channel Map +Z | 69 |

List of Figures

| | | |
|-----|--|----|
| 2.1 | The standard model of particle physics with three generations of matter fermions, gauge bosons and a Higgs boson. Figure taken from User:MissMJ et al. (2014). | 4 |
| 2.2 | Two colliding proton beam bunches, with n1 and n2 number of protons each, with idealized shape. | 6 |
| 2.3 | The cross sections and expected production rates at the LHC and the Tevatron. | 7 |
| 2.4 | Two proton bunches with more realistic profile colliding at an angle. . | 9 |
| 3.1 | Layout of CERN accelerator complex. The four LHC experiments CMS, ALICE, ATLAS, and LHCb also shown symmetrymagazine.org (2016). | 16 |
| 3.2 | Schematic of the Bunch Disposition around an LHC Ring for the 25 ns Filling Scheme Bailey and Collier (2004). 'b' and 'e' indicate beam position with or without beam. | 18 |
| 3.3 | Mean number of interactions per bunch crossing, 2012. | 19 |
| 3.4 | CMS Coordinate System with positive x towards the center of the ring. . | 20 |
| 3.5 | Relationship between polar angle and pseudorapidity. | 21 |
| 3.6 | Delivered Luminosity versus time for several years of data taking of pp collisions with the CMS detector CMS Collaboration (2016). | 22 |
| 3.7 | CMS Detector Sakuma (2016). | 23 |
| 3.8 | Schematic view of a pixel sensor Rossi (2003). | 24 |

| | | |
|------|--|----|
| 3.9 | One side of PLT telescopes and their location within CMS Hall-Wilton et al. (2009); Foerster (2015). | 25 |
| 3.10 | PLT Module. | 26 |
| 3.11 | PLT modules at forward direction(left) and backward direction (right) both located at 171 cm from the interaction point. | 26 |
| 3.12 | A schematic of the control and readout logic of Pixel Luminosity Telescope. | 27 |
| 3.13 | Bunches triggered via random trigger setup for \sim 10 lumi sections from Fill 5151 (2016) with 1579 BX cycling every 3 orbits. | 29 |
| 3.14 | Tracks which make through all 3 planes with a mask of 4mm x 4mm. | 30 |
| 3.15 | Per channel average coincidence count for 1 nibble sample from Fill 4444 (2015). | 31 |
| 3.16 | Comparison of luminosity measured via LHC beam parameters (green) and Pixel Luminosity Detector (blue) for the CMS experiment, Fill 5253. | 33 |
| 3.17 | Double Gaussian fit to PLT track rate as a function of beam separation, for bunch 1011 during the first separation VdM scan in X and Y. | 34 |
| 4.1 | Hit Display from 05-05-2015, -Z side (Ch1- Ch12). | 36 |
| 4.2 | Display of per channel 3-fold coincidences count at P5 from 05-18-2016 (-Z side). The gaussian shape represents the change in coincidence count during beam scans. | 37 |
| 4.3 | Ratio plots for NormTag validation. | 39 |
| 5.1 | 3-fold coincidence count for all channels as a function of bunch crossing, Fill 4444 (2015). | 42 |
| 5.2 | Coincidence counts for filled bunches count per nibble, Fill 4444 (2015). | 43 |
| 5.3 | Exponential drop in contribution from non-colliding bunches as a function of bunch separation from the last filled bunch. | 44 |
| 5.4 | nTracks (log) per BX, Fill 4444 (2015) at random trigger. | 45 |
| 5.5 | Reconstruction of slope-x and slope-y. | 46 |

| | | |
|-----|---|----|
| 5.6 | Reconstruction of beam spot at Z=0 plane. Ellipses drawn at 3 sigma and 5 sigma away from the mean of X, Y. | 47 |
| 5.7 | Track residuals in x, y direction for a sample run. | 48 |
| 6.1 | Different sources for tracks entering the PLT during proton-proton collisions. IP refers to interaction point and is the origin of genuine tracks responsible for luminosity. | 50 |
| 6.2 | Missing Pixel rate from Fill 4444 averaged over 5 minute interval. Missing rate from the transparent buffer is represented by +. | 52 |
| 6.3 | Number of tracks vs Beam separation, VdM Fill 4954(2016). | 54 |
| 6.4 | Slope-y from Fill 4444 with sigma cut boundaries. | 55 |
| 6.5 | SlopeX model using reconstructed tracks from vdm scan at nominal separation. | 57 |
| 6.6 | SlopeY model using reconstructed tracks from vdm scan at nominal separation. | 58 |
| 6.7 | Combined Fit to the Model. | 60 |
| 6.8 | Correction as a function of Single Bunch Instantaneous Luminosity (SBIL). The dashed line correspond to the error bars in fraction of non-lumi contribution. | 61 |
| 6.9 | Extrapolation of fit model to high accidental fractions vs the counting of the track in tails (outside 5σ) variable distributions. | 62 |

Chapter 1

Introduction

The experiments in elementary particle physics probe interactions between subatomic particles to probe the fundamental laws of nature. The standard model of particle physics is a well-tested theory that lays out the important parameters for the interaction between particles. Prediction of the existence of the top quark (1995), neutrino (2000), and Higgs (2012) have been confirmed experimentally. This model attempts to describe the electromagnetic, weak, and strong nuclear interactions among subatomic particles.

Despite its many successes, the standard model is not a complete theory. For example, gravitational interactions, the matter-antimatter asymmetry in the universe among others, is not predicted in agreement with observations by the current model. There are extensions to the SM that predict the existence of new generations of particles and forces at higher energies accessible with accelerators until recently.

Some of these ideas can be tested experimentally at the Large Hadron Collider (LHC) at CERN that collides protons at unprecedented high beam energy and intensities to produce particles of higher masses and measure rare particle reactions. At any time the precise knowledge of the rate at which proton-proton collision produce any particles, the so-called luminosity, is crucial to obtain absolute production rate of the new signals that are compared to theoretical predictions and to accurately predict

the production of fake signals that need to be subtracted. The luminosity eventually sets a limit on the confidence of our physics findings. My thesis work concerns systematic studies of the Pixel Luminosity Telescope (PLT) and the determination of background to the luminosity measurement.

This thesis documents corrections applied to the measurement of the luminosity delivered to the CMS's PLT detector at the LHC in proton-proton (pp) collisions at a center-of-mass energy 13 TeV during the 2015-2016 run period. This thesis is structured the following: Chapter 2 provides a brief overview of the standard model of particle physics and the concept of luminosity. Chapter 3 describes the experimental setup for the PLT and the method used for calibration.

CMS installed the Pixel Luminosity Telescope (PLT) in 2015; software for analyzing the machine conditions and measurement data had to be built. Chapter 4 provides an overview of operational work done as part of the thesis. Charged particle reconstruction, likelihood fits to extract signal and background contributions and corrections to the published luminosity values are discussed in chapter 5 and 6.

Chapter 2

Physics Background

2.1 Standard Model of Particle Physics

The standard model (SM) of particle physics describes the interaction between elementary particles through electromagnetic, weak, and strong forces via the exchange of force mediator particles. This model unifies theories on electromagnetic and weak interactions as published in 1961 [Glashow \(1961\)](#), with the addition of Higgs mechanism in 1967 by [Weinberg \(1967\)](#); [Salam \(1968\)](#). This theory successfully explained the experimental observations in the past and continues to provide avenues to probe the theory further.

According to the SM, matter consists of particles of spin 1/2 known as fermions each of which has its own antiparticle. These particles are treated as excitations of fields, and the forces are treated as interactions between these excitations. The interactions happen via exchange of various vector bosons, which are the particles with spin 1. There are two groups of fermions: that interact electromagnetically and weakly. The Leptons–electron, muon, tau, and their partner neutrinos only experience the electroweak force. The quarks–up, down, strange, charm, bottom, top experience both the electroweak force and the strong force. Higgs boson, with spin 0, generates the mass of particles. As the unification in the SM a priori is only valid

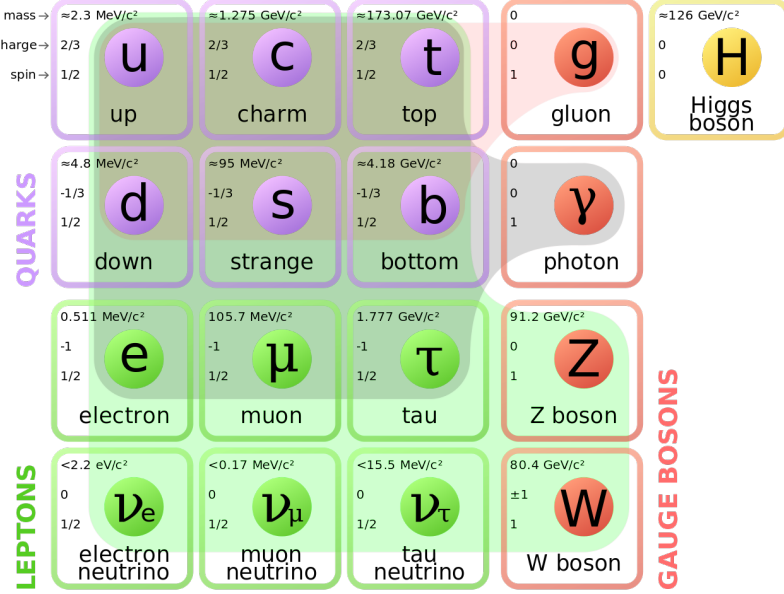


Figure 2.1: The standard model of particle physics with three generations of matter fermions, gauge bosons and a Higgs boson. Figure taken from User:MissMJ et al. (2014).

Table 2.1: Relative strengths of the four fundamental forces in terms of coupling constants. The coupling constant for each force is dimensionless.

| Interaction | Coupling constant | Strength | Mediator |
|-----------------|-------------------|------------|----------------|
| Strong | α_s | 1 | Gluon |
| Electromagnetic | α | 1/137 | Photon |
| Weak | α_W | 10^{-6} | W and Z Bosons |
| Gravitation | α_g | 10^{-39} | Graviton |

with massless particles, the Higgs mechanism is the process by which particles require mass Weinberg (1967); Salam (1968) and is mediated by the Higgs particle Englert and Brout (1964); Higgs (1964).

The particle content of the SM is summarized in Figure 2.1. Protons and neutrons that make up most of the matter around us are composed of quarks.

Despite its successes in describing particle interactions at energies accessible with particle accelerators, the SM is not a complete theory of the universe. This is among the strongest reasons to search for physics beyond the SM. During future data-taking

periods LHC hopes to push our understanding forward by observing new generations of particles and particle interaction rates that deviate from SM predictions.

2.2 Luminosity

The quantity that measures the ability of a particle collider to produce the required number of interactions is called the luminosity \mathcal{L} . Its precise knowledge is important since for many cross-sections measurements the uncertainty factor on the luminosity dominates the final result. Luminosity is the proportionality factor between the number of events per second $R(t)$ at a given time t and its production cross-section σ_P for a process:

$$R(t) = \mathcal{L}(t) \cdot \sigma_P \quad (2.1)$$

This defines the so-called instantaneous luminosity commonly measured in units of $\text{cm}^{-2} \text{s}^{-1}$. Typically running conditions vary with time t . Therefore, the luminosity of a collider also has a time dependence that needs to be carefully measured to arrive at integrated luminosity for a given data taking period which is given as:

$$\mathcal{L}_{int} = \int \mathcal{L}(t) dt \quad (2.2)$$

and measured in units of inverse barns*. The delivered integrated luminosity, which refers to the integrated luminosity which the machine has delivered to an experiment, and recorded integrated luminosity, which refers to the amount of data that has actually been stored to disk by the experiments typically differ and hence an independent measurement by the experiment is necessary.

As \mathcal{L} is process-independent it is possible to measure the luminosity with any process whose cross-section is known. For an accurate luminosity determination, however, it is essential that the process has precise theoretical predictions and at the

*1 barn = 10^{-28} cm^2

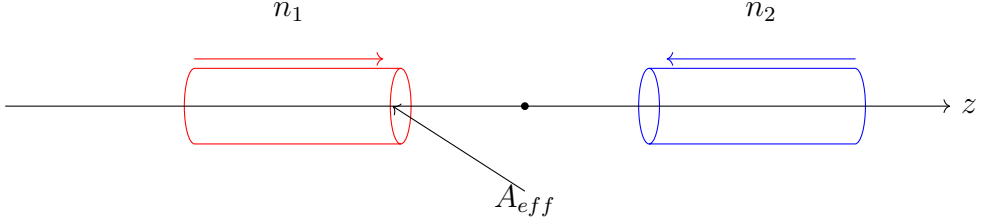


Figure 2.2: Two colliding proton beam bunches, with n_1 and n_2 number of protons each, with idealized shape.

same time that its rate can be accurately measured, i.e. enough, signal events are produced and reconstructed in a limited time interval. The production of Z^0 bosons ($pp \rightarrow Z^0 X$) that decay into leptons, particularly muons ($Z^0 \rightarrow \mu^+ \mu^-$), is such a "standard candle process", because the leptons can be well identified and theoretical prediction of the cross section has only a few percent relative uncertainty. The cross-section of Z^0 production is large enough and there are almost no fake signals.

The instantaneous luminosity can be extracted from certain beam parameters. A simplified case for a head-on collision of two bunches is shown in Figure 2.2. The luminosity can be expressed in terms of geometry and the number of particles in each of the two colliding beam bunches $n_{1(2)}$:

$$\mathcal{L} = \frac{n_1 n_2 f}{A_{eff}}, \quad (2.3)$$

with f the collision frequency. Beam parameters for the LHC are listed in Table 2.2. Of the possible 3564 bunches only $n_b = 2808$ are filled reducing the peak luminosity accordingly. The beam current $I_{1(2)}$ is given in terms of the charge of the beam particle e and the collision frequency f as $I_i = e_i f n_i$. Hence, one obtains

$$\mathcal{L}_{int} = \frac{I_1 I_2}{e^2 f A_{eff}} \quad (2.4)$$

With a nominal instantaneous luminosity of $\mathcal{L} = 10^{34} \text{ cm}^{-2} \text{ s}^{-1}$ ($= 10 \text{ nb}^{-1} \text{ s}^{-1}$) and a Higgs production cross section of $\sigma \simeq 0.1 \text{ nb}$ one expects about 1 Higgs per second. Figure 2.3 shows the cross sections for several processes at a 10 times lower nominal

proton - (anti)proton cross sections

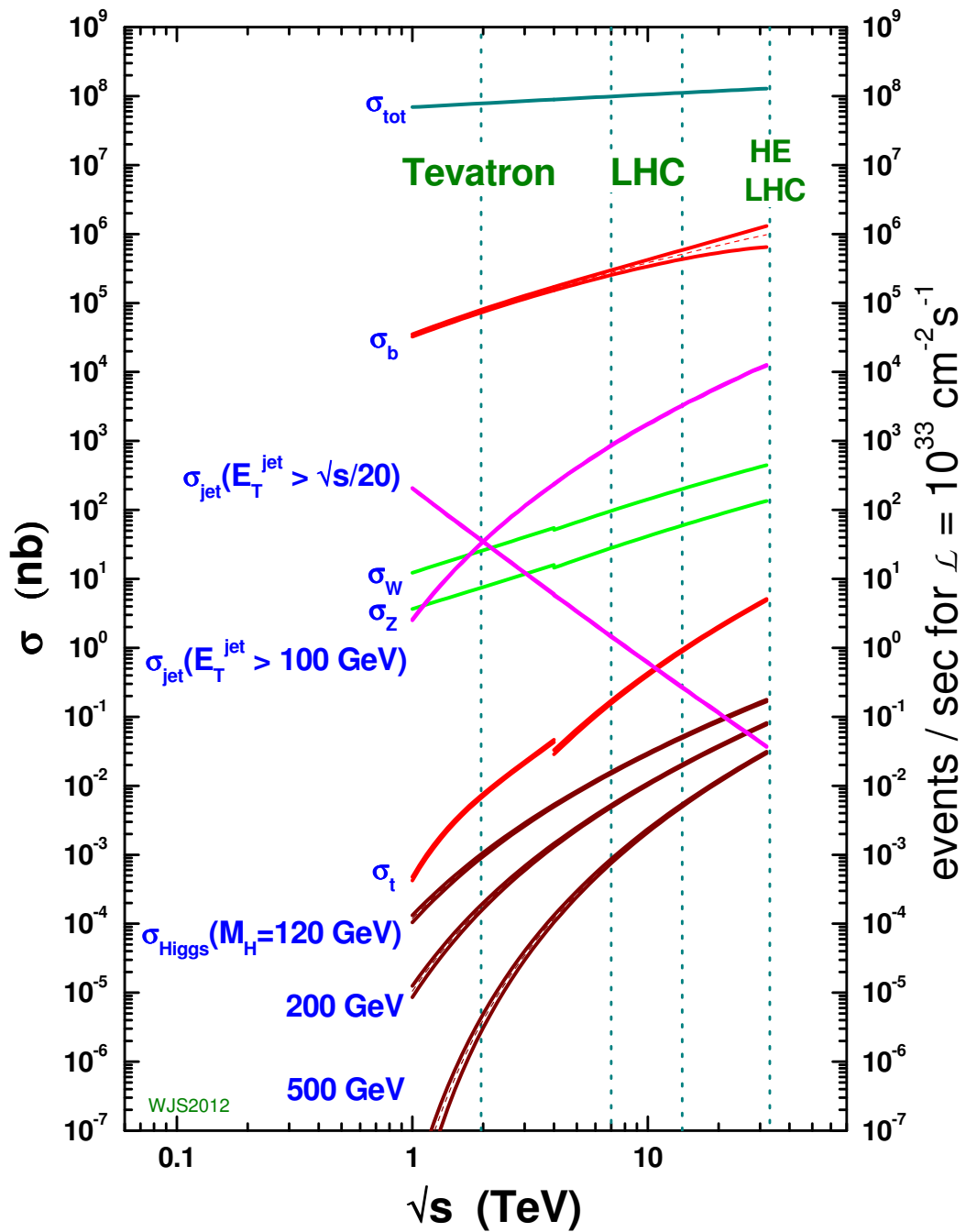


Figure 2.3: The cross sections and expected production rates at the LHC and the Tevatron.

luminosity that has been achieved so far with the LHC. At this luminosity also about 100 Z^0 particles are produced per second. Only 3.4 % of Z^0 's decay into a muon pair resulting in about 3 Z^0 particles per second that are potentially detected and reconstructed with CMS.

Table 2.2: LHC beam parameters relevant for the peak luminosity [Bailey and Collier \(2004\)](#).

| Beam Parameter | Unit | Value |
|---|------------------------|-----------------------|
| Proton Energy | [GeV] | 6500 |
| Stored energy per beam | [MJ] | 363 |
| Number of particles per bunch n_i | | 1.15×10^{11} |
| Number of bunches n_b | | 2808 |
| Bunch collision frequency f | MHz | 40 |
| Circulating beam current | [A] | 0.584 |
| Transverse beam size ($\sigma_{x,y}$) | μm | 16.7 |
| RMS bunch length (σ_z) | cm | 7.55 |
| Geometric luminosity reduction factor F | | 0.836 |
| Peak luminosity in IP1 and IP5 | [$cm^{-2} sec^{-1}$] | 10^{34} |

Assuming that the transverse profile of the two bunches distribute identically and that the profiles do not change along the bunch a good approximation is a Gaussian profile for the beam transverse distribution in x and y , each characterized with a standard deviation σ_x and σ_y , respectively. In this case $A_{eff} = 4\pi\sigma_x\sigma_y$. It implies that the profiles in x and y direction are not correlated.

The two beams at the LHC cross each other under an angle of $\theta_C = 285\mu$ rad to direct the beams after the collision into their respective vacuum pipe and to avoid multiple unwanted interactions. Figure 2.4 shows a schematic illustration of the beam crossing. It also shows a change in the profile along the beam width. The correct evaluation of the effective beam size is obtained from an overlap integral of beam density distribution functions in all three coordinates [Herr and Muratori \(2003\)](#). For small angles, Gaussian profiles and $\sigma_x \simeq \sigma_y$ in good approximation this results in the so called geometric luminosity reduction factor F, given as

$$F = \left(\sqrt{1 + \left(\frac{\theta_c \sigma_z}{2\sigma^*} \right)^2} \right)^{-1} \quad (2.5)$$

that multiplies eq. 2.3.

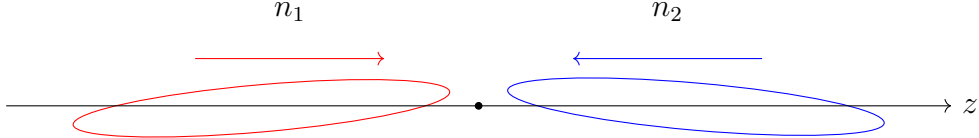


Figure 2.4: Two proton bunches with more realistic profile colliding at an angle.

In practice, however, there are complications: beams do not factorize as the profile changes over the length of the bunch and bunches do not collide exactly head-on but with offsets. Imperfections in the beam steering lead to a widening of the beam profile and therefore a reduced luminosity. So far also a uniform population of the beam bunches is assumed while in reality, the actual fill pattern can vary. The LHC provides measurements of beam currents and beam profiles along the LHC accelerator but not in the vicinity of the interaction points. Furthermore, the beam parameters and conditions change over the time period of a LHC fill. To arrive at the best time-integrated luminosity the time integral has to be taken over time intervals short enough to measure significant variations and exclude dead times. Typically the beam intensity decays exponentially with time resulting in a similar reduction in the instantaneous luminosity. The effective mean lifetime of the luminosity is further reduced by the increase in the transverse and longitudinal beam size over time. To reduce uncertainties due to extrapolation from beam parameter measurements the CMS experiment has to measure the relative luminosity with dedicated detectors and calibrate them with standard candle processes or dedicated calibration runs of the LHC.

2.3 Luminosity Calibration

One can obtain the absolute luminosity directly from beam parameters according to Eq. 2.2, without the a priori knowledge of any physics cross section. The revolution frequency f is well known and the number of particles $n_{1(2)}$ can be measured by dedicated beam charge monitors. In contrast, the transverse area of beam overlap A_{eff} is difficult to determine. Different monitors such as wire scanners or synchrotron light monitors can sample the beam profile but not close to the collision points and extrapolations lack precision. In the year 1968 Simon van der Meer proposed a method to measure A_{eff} [Van Der Meer \(1968\)](#), now known as van der Meer- (vdm-) or beam separation-scan.

Simon van der Meer proposed that it is possible to measure the profile of colliding beams by observing the counting rate R in a particle counting system while scanning the two beams vertically across each other. One of the two beams is displaced vertically with respect to the other one, and the counting rate in the monitor is plotted versus displacement. A bell-shaped curve will result with its maximum at zero displacement, then independent of beam shape A_{eff} is equal to the area under this curve, divided by the ordinate for zero displacement [Van Der Meer \(1968\)](#). At the LHC the measured counting rate depends on both horizontal and vertical beam sizes. The main assumption is that the density distributions of particles in bunches can be factorized, and two scans along the transverse planes are sufficient. If one assumes that the beam density functions are uncorrelated one can write for the counting rate R as function of displacement in x and y , δx and δy , respectively:

$$R(\delta x; \delta y) = R_x(\delta x)R_y(\delta y) \quad (2.6)$$

By scanning the two transverse planes, one obtains a direct measurement of the transverse effective beam sizes and therefore of the effective area A_{eff} :

$$A_{eff} = \frac{\int R_x(\delta x) d\delta x}{R_x(0)} \frac{\int R_y(\delta y) d\delta y}{R_y(0)} \quad (2.7)$$

The convoluted transverse width per scan direction of the two beams can be written as:

$$\Sigma_x = \sqrt{\sigma_{1x}^2 + \sigma_{2x}^2} = \frac{1}{\sqrt{2\pi}} \frac{\int R_x(\delta x) d\delta x}{R_x(0)} \quad (2.8)$$

and the same expression for Σ_y in y direction. The luminosity Eq. 2.3 becomes:

$$\mathcal{L}_{int} = \frac{n_1 n_2 f}{2\pi \Sigma_x \Sigma_y} \quad (2.9)$$

In case of a crossing angle, the vdM scan measures directly the correct effective beam size, including the effect of a crossing-angle for scans performed exactly in the crossing plane [White et al. \(2010\)](#) Figure 3.17 shows the rate of particle tracks as measured with the PLT versus the separation in the beam in x direction. The data points have been fit to a Gaussian function. A refined fit uses two Gaussian functions to achieve an improved description of the tails in the distribution.

The CMS collaboration uses the PLT detector to measure and monitor the relative luminosity. Once calibrated, one can extrapolate the absolute luminosity measurement of the vdM scan to any other luminosity scenario. With R_{inel} to be the rate of inelastic pp events, σ_{inel} the pp inelastic cross-section, f the revolution frequency of the bunches, and μ the average number of pp -collisions per bunch-crossing:

$$\mathcal{L}_{int} = \frac{R_{inel}}{\sigma_{inel}} = \frac{\mu f}{\sigma_{inel}} \quad (2.10)$$

The PLT detector with limited acceptance times detection efficiency ω will only see a subset of the events:

$$\mathcal{L}_{int} = \frac{\omega \mu f}{\omega \sigma_{inel}} = \frac{\mu_{vis} f}{\sigma_{vis}} \quad (2.11)$$

The index vis stands for visible value. Hence, the μ_{vis} can be measured and $\sigma_{\text{vis}} = \sigma_{\text{inel}}$ is practically the calibration constant to obtain the absolute luminosity. In general, this equation is valid only in the case of a linear response of the detector with respect to μ . Otherwise, corrections for the non-linearity must be taken into account.

2.4 Luminosity Measurement

The PLT detector consists of two symmetric detector arms placed on each side of the CMS interaction point (IP5). Each side is further divided into eight telescopes with each treated as separate readout channel. Particles passing through one of these telescopes are counted as a hit if their charge signals in all three detectors of the telescope are simultaneously above threshold (Fast-OR). A bunch crossing is counted as an event when there is at least one hit. The typical rate μ per bunch crossing in 2015 was 1 hit on each side respective a detector occupancy of about 0.15/BCX. Particles not originating from bunch collisions but rather collision in the beam gas and with beam halo particles result in a miscount of the luminosity and are subtracted statistically after a detailed analysis of their relative contribution. The relative contribution from such background was at most 7% in 2015. The analysis is described in detail in [Lujan et al. \(2016\)](#). The luminosity is determined by event-counting. A disadvantage of this method is that one is limited to measure either any hit or no-hit event which at high μ results in the event probability approaching one. Then every bunch crossing will be counted as an event and the method does not work anymore (is saturated).

One can derive the probability for multi-interaction events making the assumption that the number of pp interactions during a bunch crossing follows a Poisson statistics the following:

$$P_\mu(n) = \sum_{n=0}^{\infty} \frac{\mu^n e^{-\mu}}{n!} \quad (2.12)$$

where $P_\mu(n)$ is the probability to have n interactions in a bunch crossing when the average number of interactions is μ . Furthermore, the probability to detect a single interaction ω (efficiency \times acceptance of the PLT Fast-OR) is assumed not to change when several events in the same bunch crossing happen. This effect is expected to be negligible for occupancies of significantly less than 1 per bunch crossing per channel. The probability for *not* detecting a bunch crossing that has n interactions is given as:

$$P_0(n) = (1 - \omega)^n \quad (2.13)$$

With n distributed according to a Poissonian the probability to measure μ interactions when the average number is zero is:

$$P_0(\mu) = \sum_{n=0}^{\infty} (1 - \omega)^n \cdot P_\mu(n) \quad (2.14)$$

and using the expansion one obtains:

$$P_0(\mu) = e^{-\omega\mu} = e^{-\mu_{vis}} \quad (2.15)$$

With N_{OR} the number of Fast-OR events in a given time interval, and N_{BCX} the corresponding number of bunch crossings, the probability to observe a Fast-OR P_{OR} in a given bunch crossing is:

$$P_{OR}(\mu) = \frac{N_{OR}}{N_{BCX}} = 1 - P_0(\mu) = 1 - e^{\mu_{vis}} \quad (2.16)$$

From the latter two one obtains an expression for μ_{vis} :

$$\mu_{vis} = -\ln(1 - P_{OR}(\mu)) \quad (2.17)$$

The PLT obtains μ_{vis} per telescope for each of the potential 3564 bunch positions for 4096 orbits of the LHC beam corresponding to 0.365 ms. Instead of counting

N_{OR} the fraction $f_0 = (1 - N_{OR}/N_{BCX})$ of no triple coincidences in that interval is measured. This has the advantage that the multiplicity of tracks does not have to be resolved and readout only has to register signal or no signal, 0 or 1, respectively. This is the digital mode and the method is called zero-counting. The mean number of tracks per collision is then given as $\mu_{vis} = -\ln(f_0)$. The μ_{vis} is summed over all bunch crossings and averaged over all telescopes and translated into the luminosity with the calibration constant σ_{vis} . Recently, instead of averaging over telescopes, the luminosity is provided on a per-telescope basis.

Chapter 3

Experimental Setup

This chapter describes the experimental facility used in the particle physics experiments. Section 3.1 covers the Large Hadron Collider (LHC), the accelerator complex responsible for delivering pp collisions to each experiment at CERN. Section 3.2 discusses the CMS detector. The Pixel Luminosity Telescope (PLT), the dedicated online luminometer for the CMS experiment is described in Section 3.4.

3.1 Large Hadron Collider

The Large Hadron Collider (LHC), first conceived in the 1980s, is the most powerful accelerator ever built with the aim of finding Higgs boson and search for particles and forces that interact between them not included in the SM. The collider is 27 kilometers in circumference and is placed 100 meters underground at the border between France of Switzerland near Geneva.

The LHC is the last step of a multi-stage chain of accelerators called the LHC accelerator complex as shown in Fig. 3.1. Hydrogen gas atoms are stripped off electrons and the remaining protons are accelerated in the 80 m long Linac 2 linear accelerator to a kinetic energy of 50 MeV. Protons then pass through three pre-accelerators Proton Synchotron Booster (PSB), Proton Synchotron (PS), and Super Proton Synchrotron (SPS) where they are accelerated to 1.4 GeV, 25 GeV, and 450

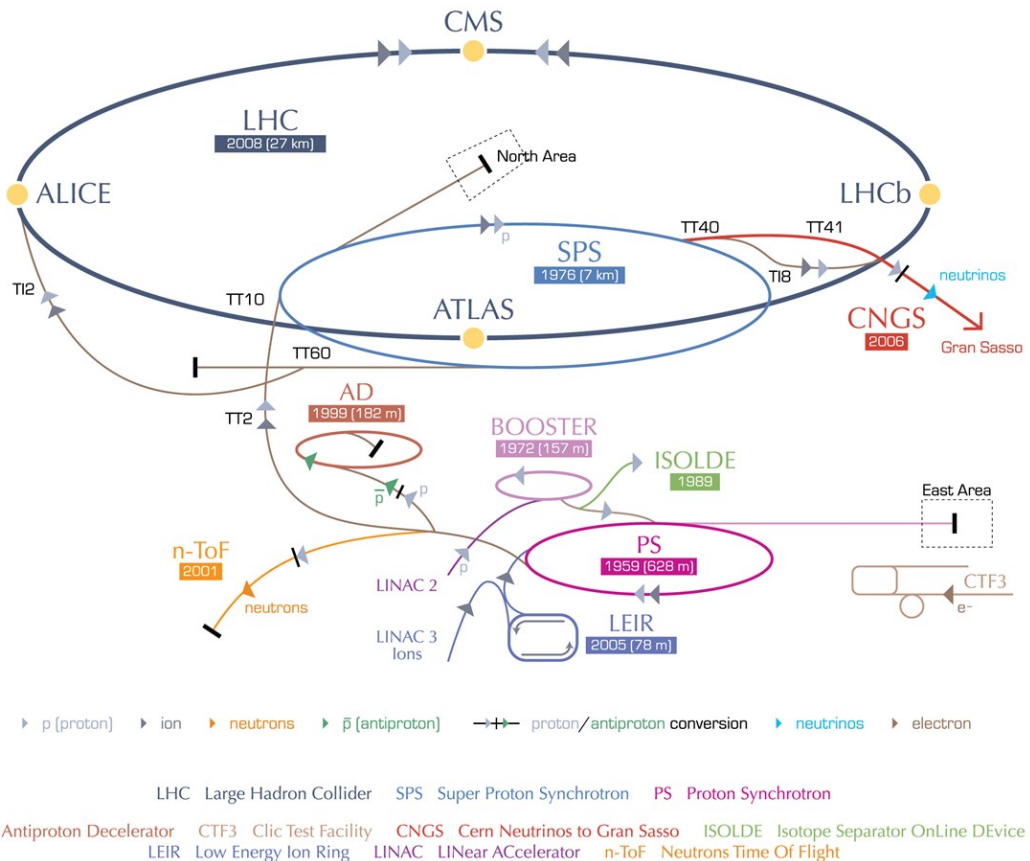


Figure 3.1: Layout of CERN accelerator complex. The four LHC experiments CMS, ALICE, ATLAS, and LHCb also shown symmetrymagazine.org (2016).

GeV, respectively. The proton beams are injected into the LHC ring where they are accelerated further to 6.5 TeV in opposite directions resulting a center-of-mass collision energy of 13 TeV.

Proton beams are segmented into groups of protons called bunches. Beams are kept on a circular path by 1232 dipole magnets located at various points around the ring. The magnetic field of 8.3 T operated at an ultracold temperature of 2 K (456 F) is generated by a superconducting coil cooled with liquid helium. Points 1, 2, 5, and 8 on the LHC ring are the interaction points where the beams overlap to produce collisions. Point 3 and 7 contain the beam collimation systems, and point 6 contains the beam dump system. The CMS experiment is located at interaction point 5.

3.1.1 Filling Scheme

Many protons are packed into each bunch to maximize the probability of a proton-proton collision for a given bunch crossing. Several filling patterns have been designed for various modes of operations of the LHC [Bailey and Collier \(2004\)](#). Typically, beams are arranged in the form of batches each with some continuous set of filled bunches.

The principle scheme for luminosity production is the 25 ns filling scheme, as shown in Figure 3.2, where each batch has 72 bunches totaling 2808 filled bunches. Gaps between the batches allow for the SPS and LHC fast injection magnets to change magnetic field, and the gap of 119 unfilled bunches at the end allows for the fast magnet that redirects the LHC beam into a beam dump to obtain full field strength. Each 25 ns bunch is confined to about 7.5 m out of the 27 km total distance in a given orbit.

3.1.2 LHC Operations in 2015 and 2016

The result described in this work is an analysis of the data taken with the Pixel Luminosity Detector for the CMS experiment during the operation of the LHC in

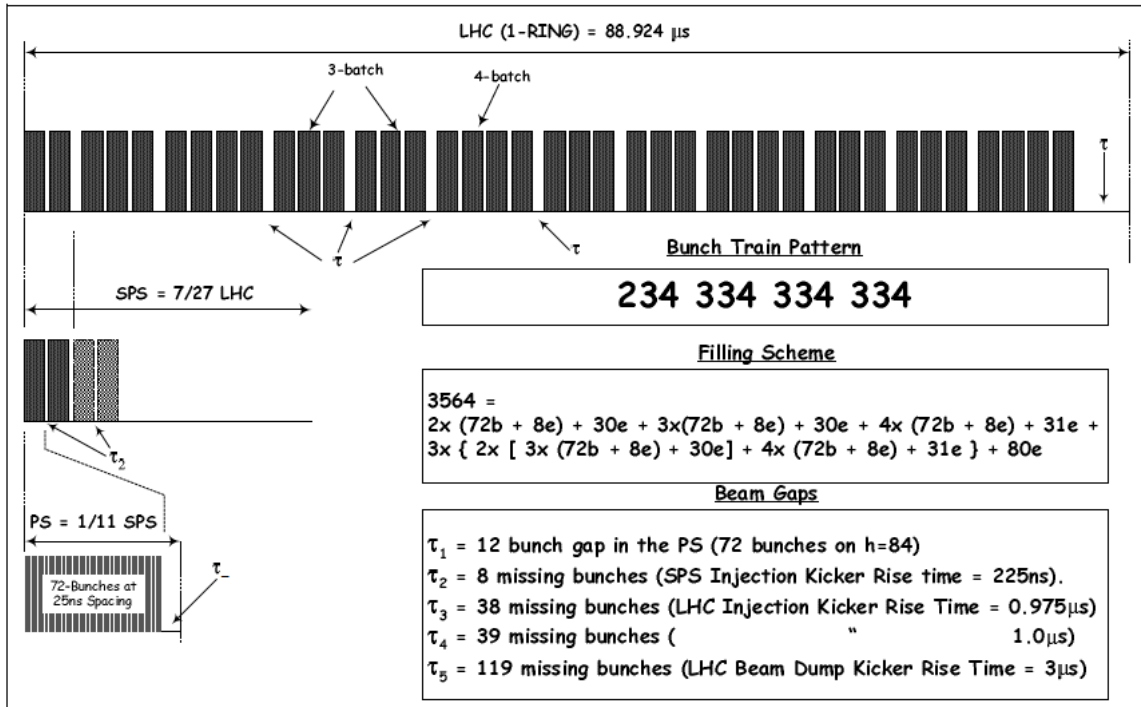


Figure 3.2: Schematic of the Bunch Disposition around an LHC Ring for the 25 ns Filling Scheme [Bailey and Collier \(2004\)](#). 'b' and 'e' indicate beam position with or without beam.

2015 and 2016. The center-of-mass energy of the pp collisions was 13 TeV. The average number of collision per bunch crossings, pileup, is shown in Figure 3.3 for this period.

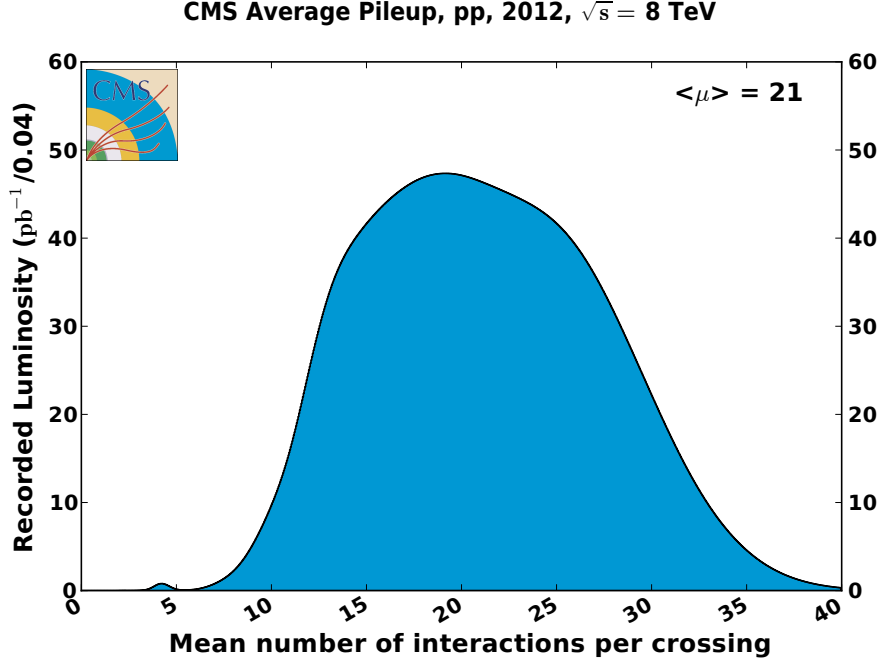


Figure 3.3: Mean number of interactions per bunch crossing, 2012.

3.2 CMS

Compact Muon Solenoid is one of two general-purpose particle-physics detectors on the LHC. It is designed to investigate a wide range of particles and phenomenon produced in the proton-proton collisions. The primary motivation for building this detector was to search for the Higgs boson and probe the standard model at energy scales above 1 TeV. This could shed some light into extensions of SM such as extra dimensions, supersymmetry , dark matter, and also gravity models around TeV scale.

The CMS coordinate system, as shown in Fig 3.4, is defined with the origin at the center of the detector. It is oriented such that the z -axis points along the LHC

ring in a counterclockwise direction, x -axis towards the center of the LHC ring, and the y -axis vertically upwards above ground.

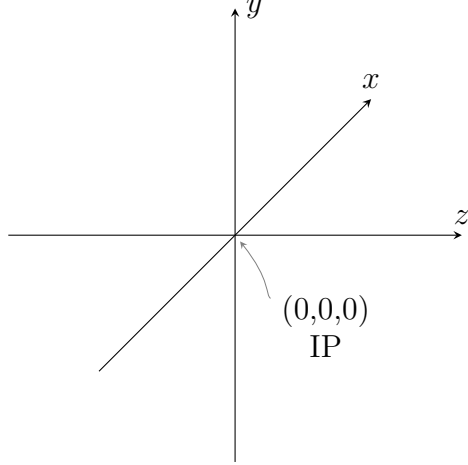


Figure 3.4: CMS Coordinate System with positive x towards the center of the ring.

In the cylindrical coordinate system, r is the radius in the $x - y$ plane, ϕ the azimuthal angle in the $+x$ direction, and θ the polar angle in the $+z$ direction. The four-momentum of a particle can be written as

$$p = \begin{pmatrix} E \\ \vec{p} \end{pmatrix}$$

where $\vec{p} = (p_x, p_y, p_z)$ in cartesian basis. The transverse momentum p_T in $r - \phi$ plane is given by

$$p_T = \sqrt{p_x^2 + p_y^2}$$

Particle kinematics can then be described by azimuthal angle, transverse momentum, and rapidity, y . Rapidity is additive under Lorentz transformations along the z axis and is given by

$$y = \frac{1}{2} \ln \left(\frac{E + p_z}{E - p_z} \right)$$

For relativistic particles, the rapidity equals the pseudo-rapidity η , which is related to the particle polar coordinate by the following relation

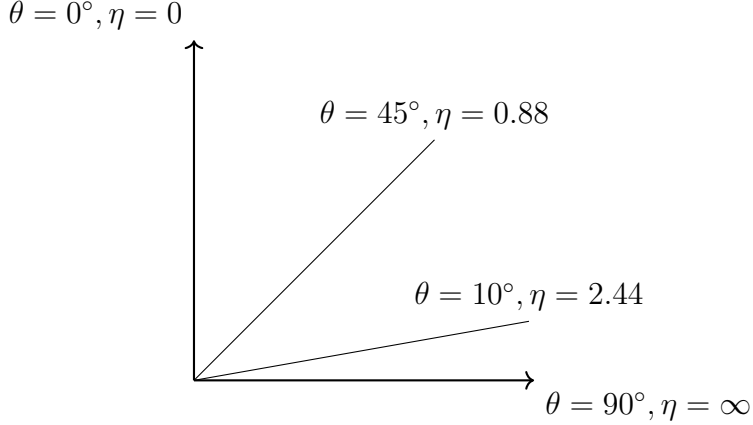


Figure 3.5: Relationship between polar angle and pseudorapidity.

$$\eta = -\ln(\tan(\theta/2))$$

The central feature of the CMS apparatus is a superconducting solenoid of 6 m internal diameter, providing a magnetic field of 3.8 T. Within the superconducting solenoid volume are a silicon pixel and strip tracker, a lead tungstate crystal electromagnetic calorimeter (ECAL), and a brass and scintillator hadron calorimeter (HCAL), each composed of a barrel and two endcap sections. Forward calorimeters extend the pseudorapidity [Collaboration \(2008\)](#) coverage provided by the barrel and endcap detectors. Muons are measured in gas-ionization detectors embedded in the steel flux-return yoke outside the solenoid.

Precise position measurement of charged particles coupled with a strong magnetic field of the solenoid provides the parameters necessary for momentum resolution. The Electromagnetic Calorimeter and Hadronic Calorimeter provide the energy resolution. The Muon System and the silicon tracker measure the charged muon and inclusive particle positions respectively. The silicon tracker measures charged particles within the pseudorapidity range $|\eta| < 2.5$. It consists of 1440 silicon pixel and 15,148 silicon strip detector modules and is located in the 3.8 T field of the superconducting solenoid. For nonisolated particles of $1 < p_T < 10 \text{ GeV}$ and $|\eta| < 1.4$, the track resolutions are

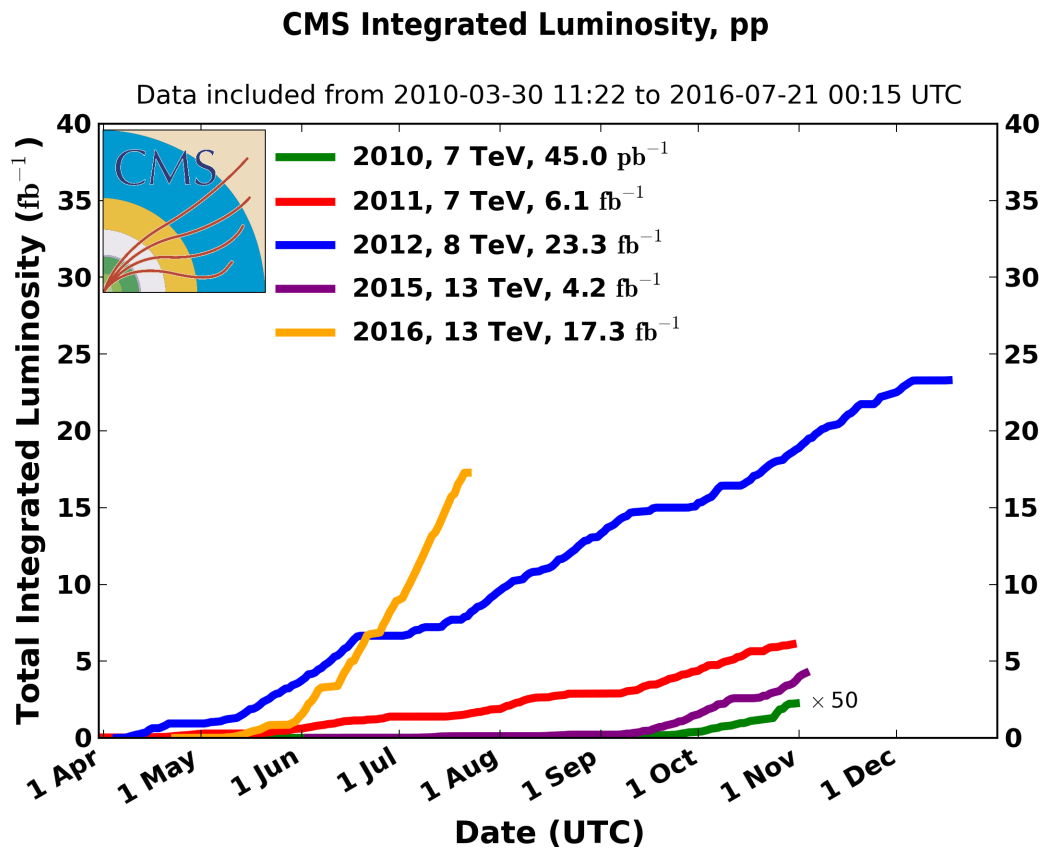


Figure 3.6: Delivered Luminosity versus time for several years of data taking of pp collisions with the CMS detector [CMS Collaboration \(2016\)](#).

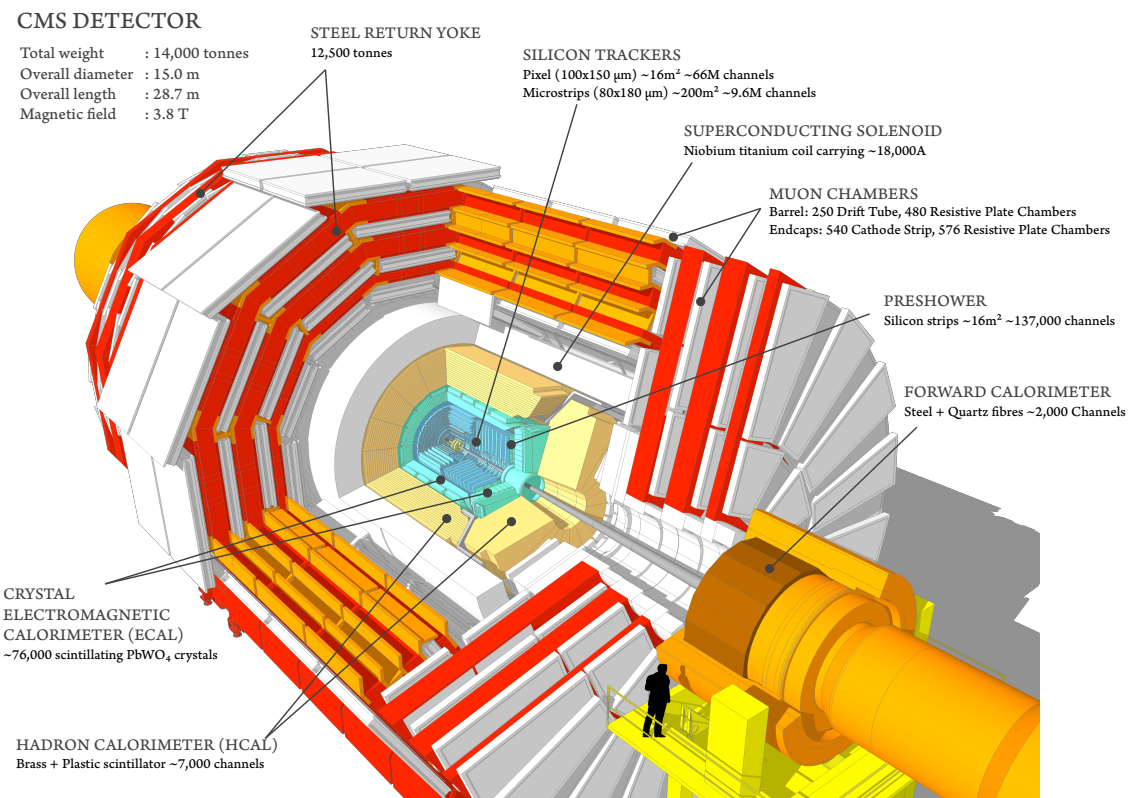


Figure 3.7: CMS Detector Sakuma (2016).

typically 1.5% in p_T and 25–90 (45–150) μm in the transverse (longitudinal) impact parameter Chatrchyan et al. (2014). A more detailed description of the CMS detector, together with a definition of the coordinate system used and the relevant kinematic variables, can be found in Ref. Collaboration (2008).

3.3 Silicon Pixel Detectors

Pixel detectors are used to measure increasing number of charged particles at high energies in particle physics experiments. As the name suggests, silicon sensor is segmented into smaller pixel elements because of which events can be identified with high space and time resolution. As such, these detectors are also an excellent choice to study short-lived particles.

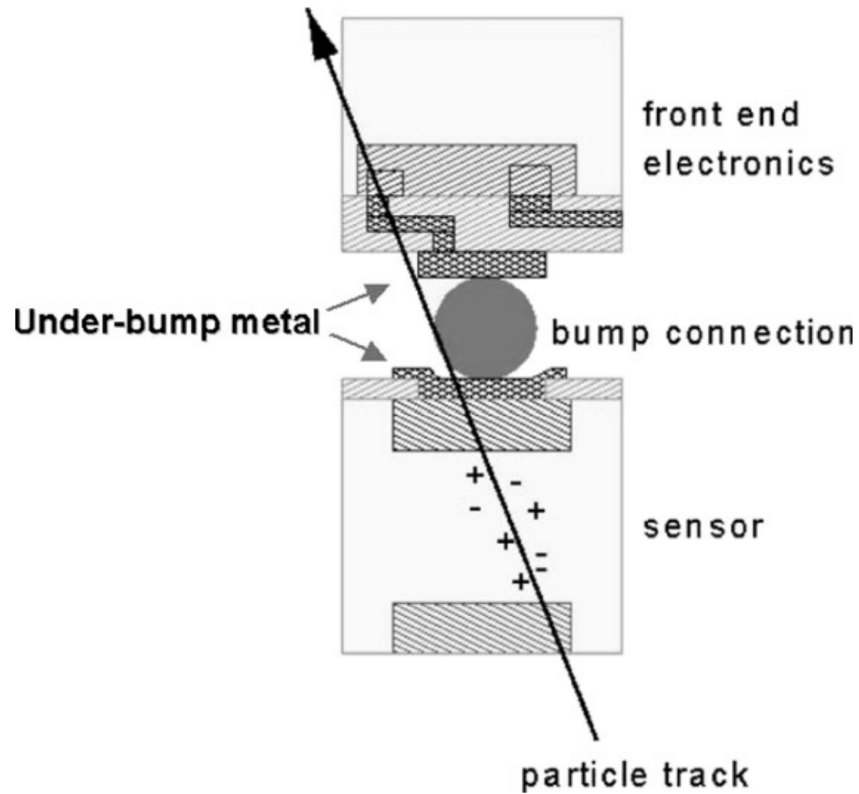


Figure 3.8: Schematic view of a pixel sensor Rossi (2003).

The sensor element of the pixel detector is typically few mm^2 . For silicon sensors in particular, about 3.6 eV energy deposition produces an electron-hole pair. The charges produced by the traveling charged particle on the silicon sensor is collected using an external electric field produced by a reverse-biased pn junction. This provides the electric field required to collect the charges formed and also suppresses the free charges. Figure 3.8 shows the schematic of building blocks of a pixel detector.

3.4 Pixel Luminosity Telescope

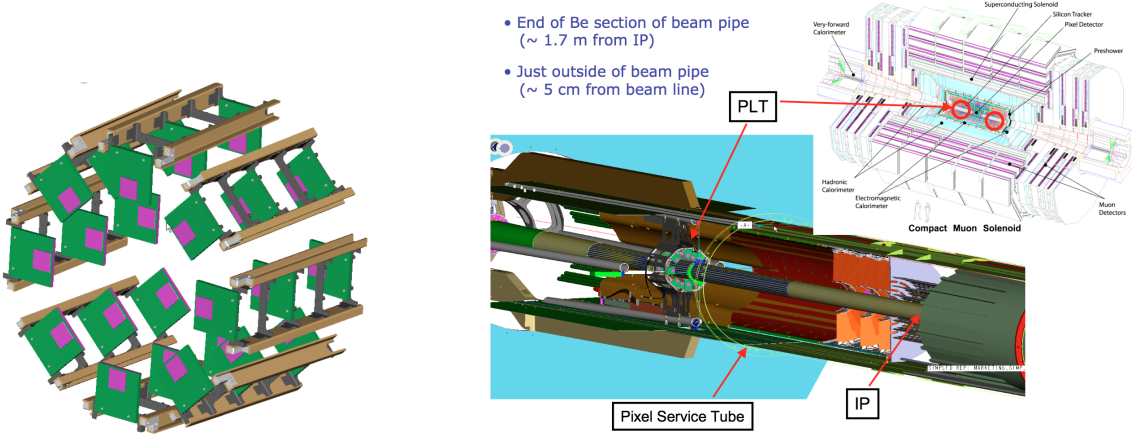


Figure 3.9: One side of PLT telescopes and their location within CMS [Hall-Wilton et al. \(2009\)](#); [Foerster \(2015\)](#).

The Pixel Luminosity Telescope is a dedicated system for measuring the luminosity at CMS using silicon pixel sensors [Kornmayer \(2015\)](#). The instrument is positioned close to the beam pipe and directly behind the Forward Pixel detector. It is designed to provide bunch-by-bunch luminosity measurement at the CMS interaction point. It is located at a pseudo rapidity, $|\eta|$, of roughly 4 and at a mean radial distance of ~ 5 cm from the beam. It was installed in January 2015 as part of the Run 2 upgrades for the CMS Beam Radiation Instrumentation and Luminosity (BRIL) project [Dabrowski \(2014\)](#), and has operated successfully throughout the 2015 and 2016 run of the LHC.

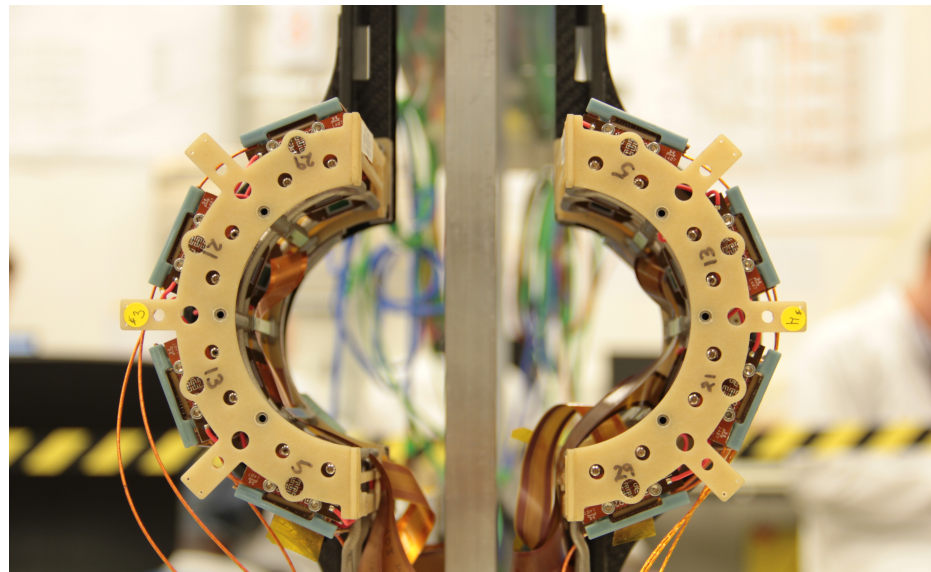


Figure 3.10: PLT Module.

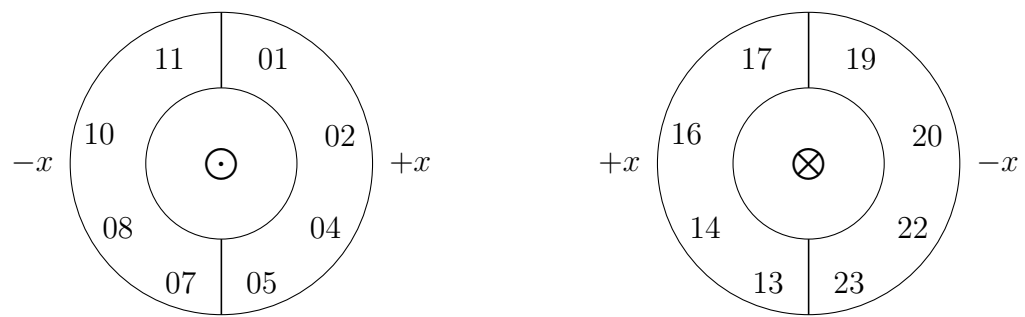


Figure 3.11: PLT modules at forward direction(left) and backward direction (right)
both located at 171 cm from the interaction point.

The PLT consists of a forward and backward module with each having 8 telescopes. Each telescope consists of 3 consecutive planes of silicon pixel detectors spaced apart by 3.75 cm. Each pixel sensor is segmented into of 80 rows and 52 columns of pixels, with each pixel $150 \mu\text{m}$ wide and $100 \mu\text{m}$ high for a total active area of about $8 \times 8 \text{ mm}^2$. The middle plane is placed 0.102 cm higher than the first plane, and the third plane is placed 0.102 cm higher than the middle plane to maintain an average viewing angle of 0.27 degrees toward the interaction point.

Read Out Chip (ROC)

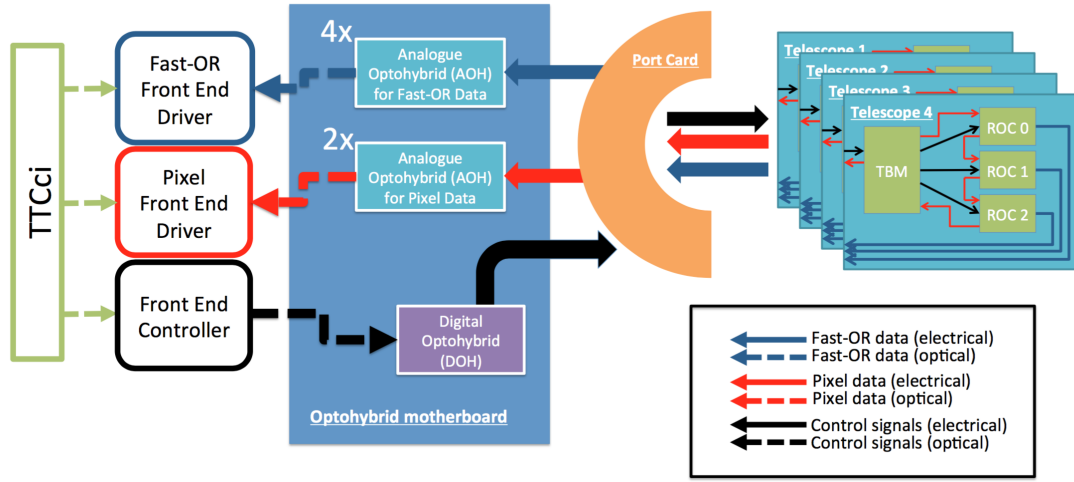


Figure 3.12: A schematic of the control and readout logic of Pixel Luminosity Telescope.

The sensors are read out by a PSI46v2 readout chip (ROC), the same that is used in the CMS pixel detector Kästli et al. (2006); Gabathuler (2005); Barbero (2003). Each ROCs from each telescopes are connected to a HDI card, which contains the Token Bit Manager (TBM) chip that handles the readout of the series of ROCs Bartz (2005). A port card, which manages the communication and control signals, is connected to half of the telescopes in each side which is then connected to opto-motherboard which converts the electrical signals into optical signals. The four

telescopes connected to a single port card are identified by their hub number, which are (in clockwise order) 5, 13, 21, and 29 as shown in Appendix Table. A.1 and A.2.

Data Streams

The front-end readout electronics consist of a FEC (Front-End Controller) card, which issues commands to the ROCs Allkofer et al. (2008), and three FED (Front-End Driver) cards Pernicka et al. (2007). One FED is responsible for the readout of the pixel data from the ROCs and is identical to the FEDs used by the pixel detector. The other two FEDs (one for each side of the detector) read out the Fast-OR data from the ROCs.

The pixel data Barbero (2003) is read out via Slink and saved to disk on a dedicated computer hard drive, while the Fast-OR data is collected in a histogram with the FED. The histogram contains a bin for each bunch crossing (BX) and is incremented by 1 in case a telescope found at least 1 signal count for each sensor. The counts within the bins are added for every 4096 orbits (lumi nibble) corresponding to a time interval of about 13. ms. The integration occurs via a VME PC which is connected to the FED via an optical bridge.

Fast-OR Data

The 52 columns in a sensor are segmented into a group of double columns, 0-26. Each hit on a double column is registered as a signal. For a given bunch crossing, the hits in double columns per sensor are reported to the FED which tests if there was at least one signal in each of the three planes. This triple-coincidence count rate is translated to luminosity value as described in sec 3.4.2.

Pixel Data

Each pixel of a sensor is calibrated beforehand where some amount of charge collected can be translated to some number of hits. Once a sensor registers a charge signal above some threshold value, the pulse height, and pixel address together with the timestamp information is saved to a buffer. Once the pixel detector receives a valid external signal trigger, the information is transferred to the FED via optical connections.

Trigger

The rate of collision, proportional to LHC bunch crossings of 25 ns, translates to a frequency of 40 MHz. A trigger is used to reduce the amount the data to a more manageable rate. To this end, two different approaches were employed: a trigger generated by taking an OR of the fast-or coincidence signals from all of the channels was used in the early 2015 run to maximize the pixel data taken. It means that if any of the channels registered a triple coincidence for a BX, FED looked for hit signals for that BX. Starting late 2015, a purely random trigger at a rate of 2 kHz was used to avoid any systematic uncertainties in the trigger that could have been introduced by our choice of using fast-or signals for trigger signals.

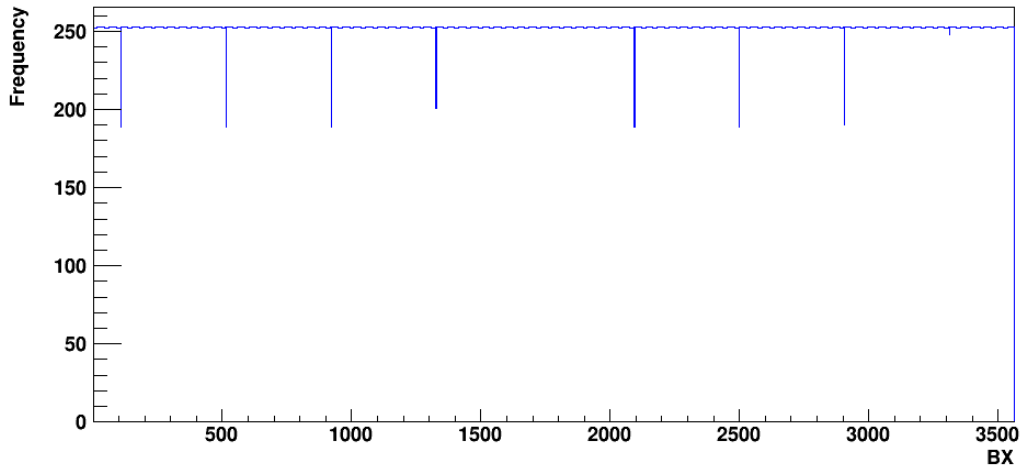


Figure 3.13: Bunches triggered via random trigger setup for ~ 10 lumi sections from Fill 5151 (2016) with 1579 BX cycling every 3 orbits.

TTCci hardware supports internal random trigger or a fixed sequence of intervals [TTCci User Guide \(2007\)](#). In order to achieve a sufficiently random trigger within 3564 bins and achieve a manageable rate of 3 kHz, the trigger is made to advance by 1585 bunches every 3 orbits (out of 4096 per nibble). Fig. 3.13 shows the BXes triggered via random trigger setup for the Fill 4444 from September 30, 2015. One downside of having a random trigger approach is that pixel data gets saved at a high rate even when there is no beam.

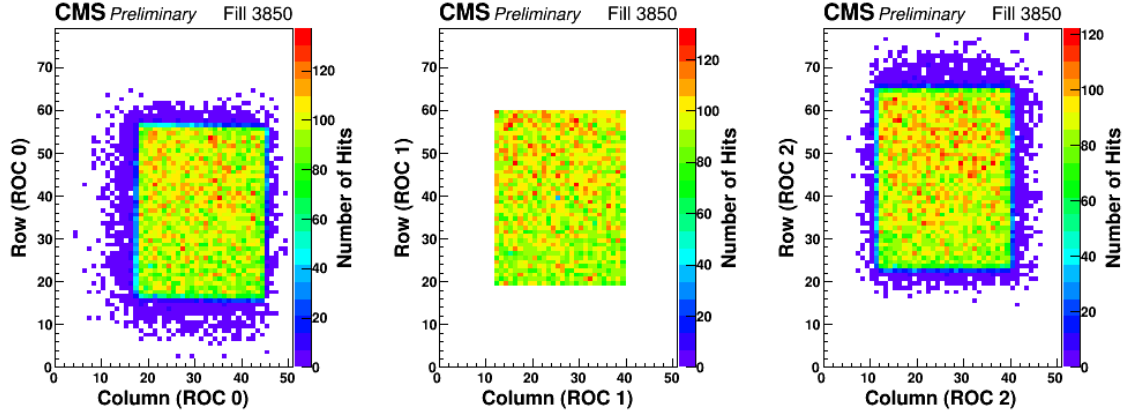


Figure 3.14: Tracks which make through all 3 planes with a mask of 4mm x 4mm.

3.4.1 Triple coincidence measurement

Real tracks are assumed to hit all three planes in a given telescope. In other words, the magnetic field has little effect on the trajectory of particles hitting the telescopes. The fast-or data is saved in a histogram where each bin is separated by 25 ns bunch spacing. Each bin of the histogram records the number all the triple coincidences on all three planes for each telescope over a 1 lumi-nibble which is 4096 orbits.

Figure 3.14 shows the occupancies in a single telescope of the Pixel Luminosity Telescope (PLT) with a mask applied to reduce the active area of the central plane to 4mm x 4mm. This plot shows only events where a triple coincidence (a simultaneous hit in all three planes) occurred in this specific telescope, allowing us to measure the effects of alignment and accidentals.

In order to decrease the contribution from combinatoric effects producing fake triple coincidences, the active area of the sensors was decreased by masking out outer pixels. The center plane of each telescope was reduced to an active area of 4.2x4.0 mm (28 columns x 40 rows) and the outer two planes to 5.4x5.2 mm (36 columns x 52 rows).

During early commissioning operations, Channels 22 and 23 in Fig. 3.11, stopped responding and were dropped from the luminosity calculations. One more telescope, Channel 1 also was taking out of the calculation in 2016 data taking period.

3.4.2 Zero Counting Algorithm

The average occupancy of the PLT at the LHC design luminosity is about 0.1 per BX. For a given telescope, the number of hits that it receives in a bunch crossing can be considered a simple counting experiment. Figure 5.1 shows the mean number of coincidence count per telescope for a sample data.

The number of hits is proportional to the length of the interval, which is 25ns in our case. The probability of occurrence of two or more hits is very small and the number of events for one bin is independent of what happens in another bin. As such, the triple-coincidence count can be treated as a problem in Poisson statistics as described in sec 2.4.

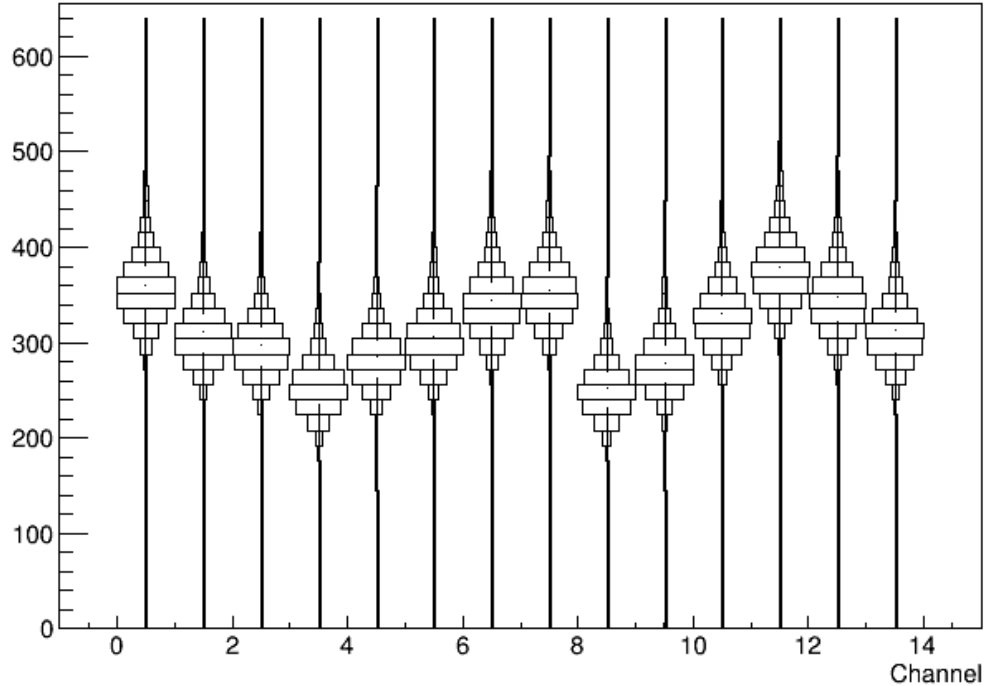


Figure 3.15: Per channel average coincidence count for 1 nibble sample from Fill 4444 (2015).

3.4.3 Van der Meer Scan Calibration

The Van der Meer (VdM) scans procedure [Van Der Meer \(1968\)](#) is used to measure the conversion factor between the number of tracks measured by the PLT and the delivered luminosity as described in 2.3. The LHC performed the VdM procedure for CMS on 24th August 2015 (LHC Fill 4266), and on 27th May 2016 (LHC Fill 4954)

The relationship between the instantaneous luminosity provided by the LHC and the mean number of tracks per bunch crossing, μ_{tracks} , is given by

$$\frac{dL}{dt} = \frac{\mu_{tracks} f}{\sigma_{vis}}$$

Where f is the LHC revolution frequency of 11,246 Hz and σ_{vis} is the fraction of the total inelastic cross-section of CMS visible to the PLT. One can then determine σ_{vis} via the VdM procedure, as described in section 2.3 and 2.4, using only the LHC beam parameters as follows:

$$\frac{dL}{dt} = \frac{I_1 I_2 f}{2\pi\sigma_x\sigma_y}$$

Here, I_1 and I_2 are the measured beam currents, and σ_x and σ_y are the beam width parameters along the x and y-axes. The LHC Fast Bunch Current Transformers (FBCT) and beam Quality Monitoring (BQM) independently provide a bunch-to-bunch measurement of beam currents. The measured current over bunches is then normalized to the total current by the Direct-Current Current Transformers (DCCT). Figure 3.16 shows a comparison of the luminosity measurement via LHC parameters and Pixel Luminosity Detector for the CMS experiment [Lujan et al. \(2016\)](#).

σ_x and σ_y are derived from fits of the observed number of PLT Fast-OR as a function of the beam separation. For each of the five scan pairs, the beams are moved between $+6\sigma$ and -6σ in steps of 0.5σ . Each fit can then be performed on the resulting 25 data points. As the beam has been found to be non-Gaussian to a degree, the fit is performed using a combination double-Gaussian function

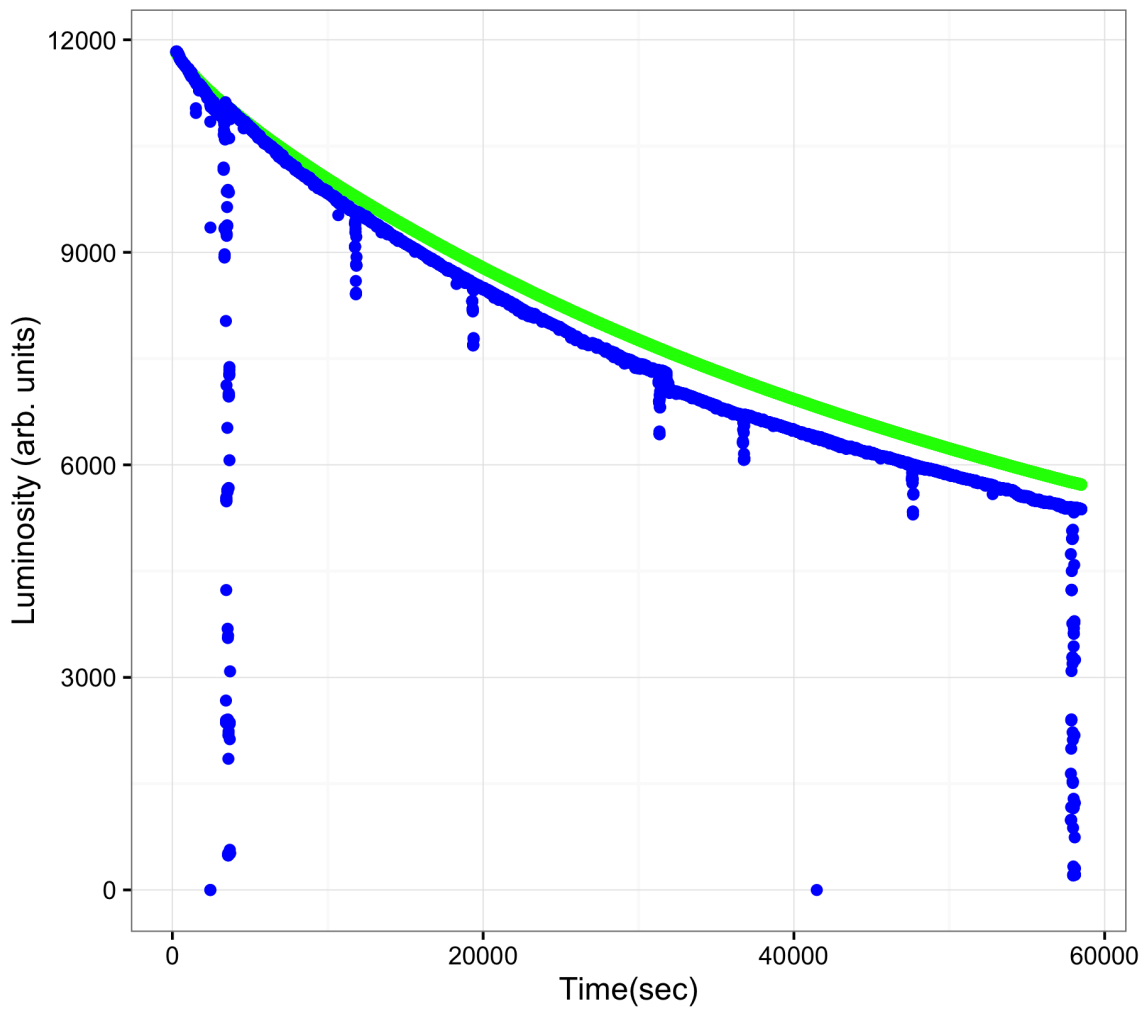


Figure 3.16: Comparison of luminosity measured via LHC beam parameters (green) and Pixel Luminosity Detector (blue) for the CMS experiment, Fill 5253.

$$R(\Delta_{x/y}) = a_1 \exp\left\{ \frac{-(\Delta_{x/y} - \mu)^2}{2\sigma_1^2} \right\} + a_2 \exp\left\{ \frac{-(\Delta_{x/y} - \mu)^2}{2\sigma_2^2} \right\}$$

where the means of each Gaussian are constrained to be equal, and the effective constant a_{eff} and effective width σ_{eff} are given by:

$$a_{eff} = a_1 + a_2$$

$$\sigma_{eff} = \frac{a_1\sigma_1 + a_2\sigma_2}{a_1 + a_2}.$$

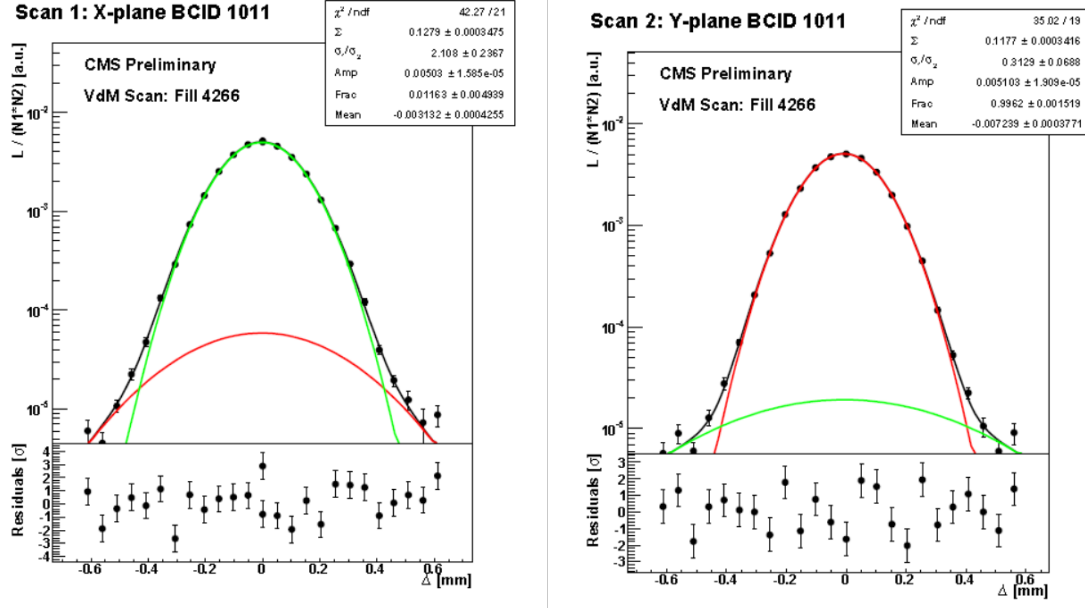


Figure 3.17: Double Gaussian fit to PLT track rate as a function of beam separation, for bunch 1011 during the first separation VdM scan in X and Y.

The final conversion factors extracted via the vdm scan for 2016 is 328 inverse microbarns/second with an uncertainty of 5%.

Chapter 4

Operations of PLT

4.1 Introduction

PLT is the youngest detector for the BRIL system dedicated to providing online luminosity. Having been installed in 2015, a lot of infrastructures had to be built for the operation of PLT from ground up. This chapter explains some of the operational work done for the PLT as part of the thesis. Section 4.2.2 gives an overview of reconstructed pixel hits seen from the CMS coordinate system. Section 4.3 discusses some of the operational issues PLT encounters and the work was done to detect and correct those problems. Section 4.4 and section 4.5 give an overview of data handling and data housing for record keeping purpose.

4.2 Machine condition monitoring

4.2.1 Hit Display

Early data from Slink was analyzed offline to look at the coordinate positions of individual hits that are recorded by each plane. Fig. 4.1 shows the hits on each plane of a telescope for -Z side from Fill 3679 which was taken on June 5, 2015. It serves as

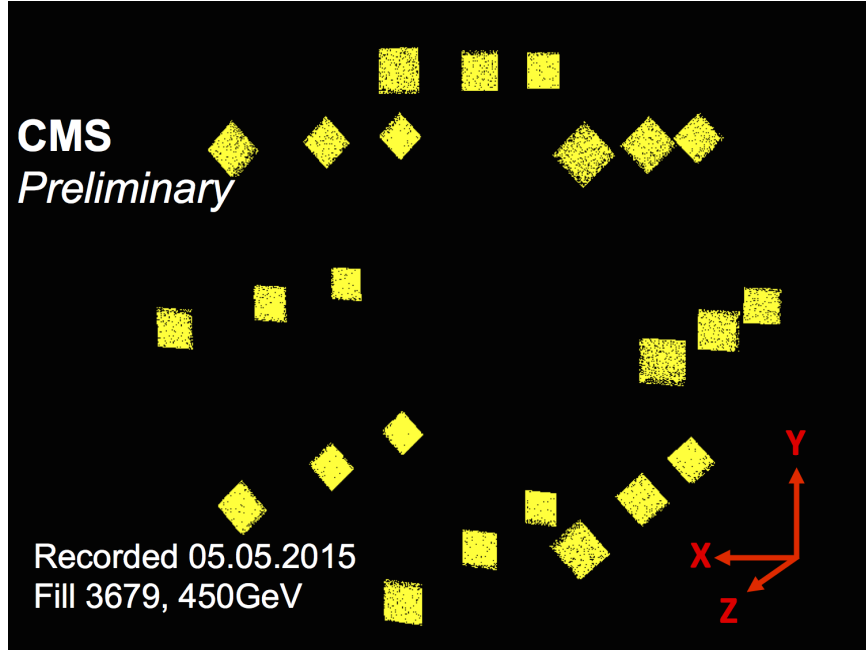


Figure 4.1: Hit Display from 05-05-2015, -Z side (Ch1- Ch12).

a sanity check for telescope alignment and it is also reassuring to see each pixel hits visually in a global coordinate system.

4.2.2 Coincidences count

BRIL group has a station in p5 where a shifter looks at data being taken by multiple luminometers (PLT, HF, BCMHF) and reports any abnormalities during the data taking process. It is important to identify and fix fatal communications defect associated with detector electronics and/or data taking as soon as such event happens.

A script was written to read data off data streams from the machine close to the detector. This was then used to make a live display of data coming from different detector channels. This code is deployed to the p5 station at CERN, the closest point to a detector and data warehouse where data gets saved downstream for the record. This display lets users know the operational condition of the machine in a more interactive and user-friendly manner. Fig. 4.2 shows the plot of live coincidence counts for each telescope for the PLT.

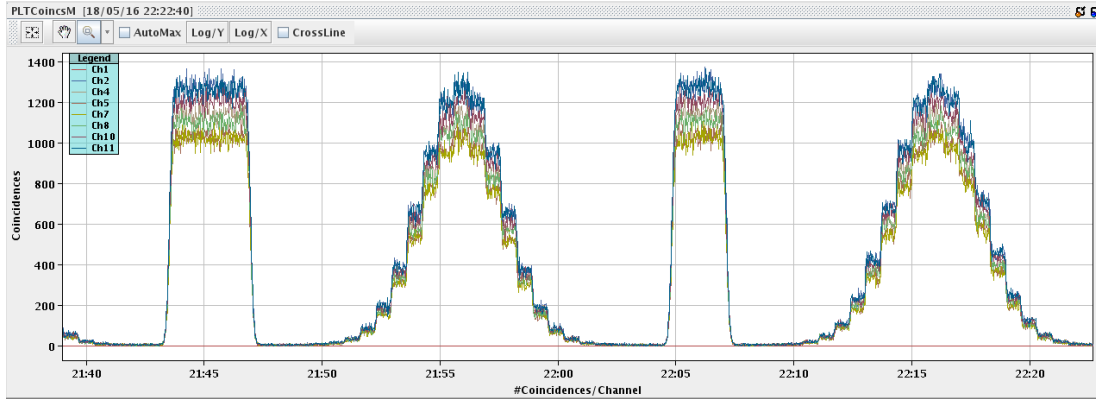


Figure 4.2: Display of per channel 3-fold coincidences count at P5 from 05-18-2016 (-Z side). The gaussian shape represents the change in coincidence count during beam scans.

4.3 Alarm Mechanism

A major part of the operation is to know exactly what is going on with the detector. Some channel could be behaving erratically, channel(s) have dropped out, a quadrant isn't sending data, baseline drift or something else could be happening. Since PLT is a dedicated online luminometer, it is important to know the status, and report any operational issues to the available experts as soon as events happened.

It is not always feasible to have a shifter at p5 for all the data taking process. Automatic alarm mechanism was deployed using PLTAnalyzer script, which takes a running average of the coincidence counts for each channel and reports errors for prompt diagnostics of detector components. Following is a tentative rundown of algorithm used for sending alarms:

- Check if coincidence count for channels is greater than some threshold value.
This eliminates spurious alarms during non-stable beams.
- Check if TCDS data makes sense. Often this causes large coincidence counts to lump into 1 particular nibble that causes spikes in lumi.
- Save the coincidence count for each channel from last N lumi sections to a 2d vector

- Get the average of N lumi sections, compare it to sum from this lumi section
- Get the % deviation from average for each channel
- Find the deviation from the average deviation for each channel. This eliminates alarm to when all channels rise up or fall down similarly.
- Assign a threshold for a channel to go up or down in each lumi section. Send alarm if a non-zero number of channels deviate from average deviation.

If an alarm criterion is met, per channel coincidence count from the current lumi section, average from last n lumi sections for each channel, and other statistics is saved to a log file for future reference. An email is also sent to users if alarm conditions are met so that operational issues are dealt with promptly.

4.4 Elastic Search - Data warehousing

Data saved to Slink or Histogram files from fast-or take huge amount of time to analyze just because of the sheer size of the dataset itself. It is desirable to have a system where one can save some representative data at a lower rate that can be queried/searched to look for patterns in data. One might be interested in knowing coincidence count as a function of Fill, lumi section, day, or any other relevant parameter.

Data is sent to elastic search database at a less granular level. The data gets saved to the database for some time which can be accessed for diagnostic purpose. See Appendix ?? for relevant part of the code within PLTAnalyzer.cc.

4.5 Data Validation

BRIL group also has other luminometers that make luminosity measurement by other methods. After getting the data, an expert generally inspects the data and assigns

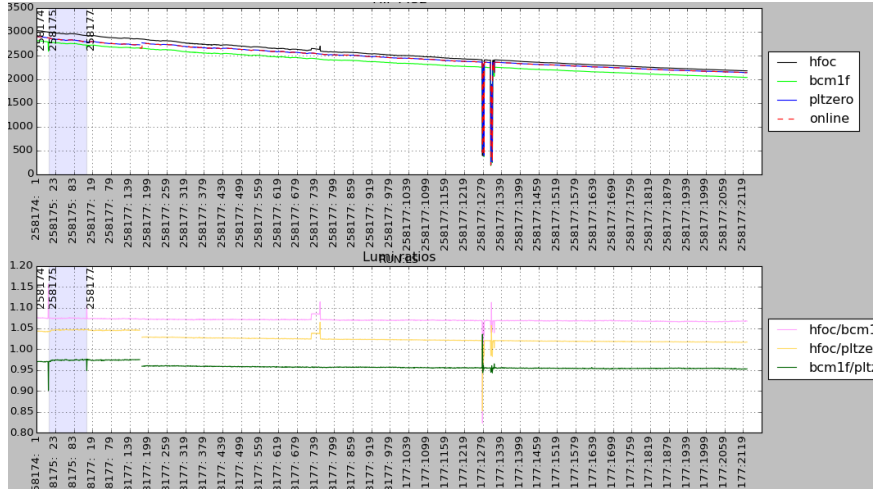


Figure 4.3: Ratio plots for NormTag validation.

good/bad tags to it. PLT, for example, could have had a channel drop out for a fill, run number, and lumi section rendering the data taken useless. It is not feasible for users to make plots to all data and comb through each lumi section for any peculiarities. A code was written to make things easier for users to identify and flag bad data regions. Make ratio plots to find agreement or disagreement with other luminometers.

Chapter 5

Event Reconstruction

PLT reports the online luminosity value by using the fast-or dataset. Slink data is used offline to parametrize the events and look for corrections to be applied to the luminosity value. In this chapter, reconstructions of events from each PLT data streams is described. Section 5.1 describes the method used to find the correct alignment of each telescope which is done before track reconstruction. Section 5.2 and section 5.3 describe the reconstruction of event from fast-or and slink data.

5.1 Telescope Alignment

PLT data is saved in granular level via the slink streams for offline analysis. Each hit is saved according to its channel number, bunch number, plane number and the pixel within the plane. In the plane's coordinate system, each pixel can be identified by its row and column number where each row is $150\mu m$ and each column is $100\mu m$. This is akin to just the first quarter of cartesian coordinate system with $(0, 0)$ representing plane's leftmost pixel from the lowest row.

Each telescope's position with respect to the CMS coordinate system is known beforehand. In the telescope coordinate system, midpoints of planes 0, 1, 2, are positioned at $(0, 0, 0)$, $(0, 0.102, 3.77)$, and $(0, 0.204, 7.54)$ respectively. Hit positions

from each plane are then translated to the CMS coordinate system with (0, 0, 0) at the interaction point to look for patterns in measurement data.

A set of hits that pass through all three planes and assumed to be the trace of a moving charged particle are referred to as tracks. This is analogous the triple coincidence criteria set for fast-or but with few differences. Unlike fast-or, which uses the zero-counting algorithm, tracking algorithm is designed to make multiple tracks from the set of hits and clusters of hits in plane 0, 1, and 2.

For alignment purpose, only the "cleanest" set of tracks are considered, namely the tracks with only 1 hit in plane 0, 1, and 2 each. As a reference, the "ideal" alignment file is used and the tracking algorithm is applied to sets of hits passing the triple-hit criteria. Under the ideal assumption, a good track would hit same pixels (rows, columns) in each plane shifted by the predefined alignment of the PLT planes. Tracking algorithm makes the best fit to the three hits in each plane of a telescope, and the residuals are calculated for each such tracks. This step is repeated for a large number of tracks and the deviation from the ideal alignment is calculated to generate a final translated alignment file for each data taking period.

5.2 Fast-or triple fold coincidences

Fast-or data stream saves coincidence count for each channel in a form of histogram where the bunch is the bin number. Each histogram gets cleared every nibble (4096 orbits) and sent downstream to be converted to a luminosity value. For each orbit, depending on the number of bunches that are made to collide, each telescope is likely to receive only a few triple-coincidences. Figure 5.1 shows coincidence count for all telescopes for Fill 4444 from 2015 in a logy scale, with tall bins representing the filled bunches.

For every bunch crossing, only ... are likely to collide as seen in Figure 3.3. Out of those colliding particles, PLT is expected to receive only some because of the detector's rapidity location, and acceptance region. Each histogram for a given

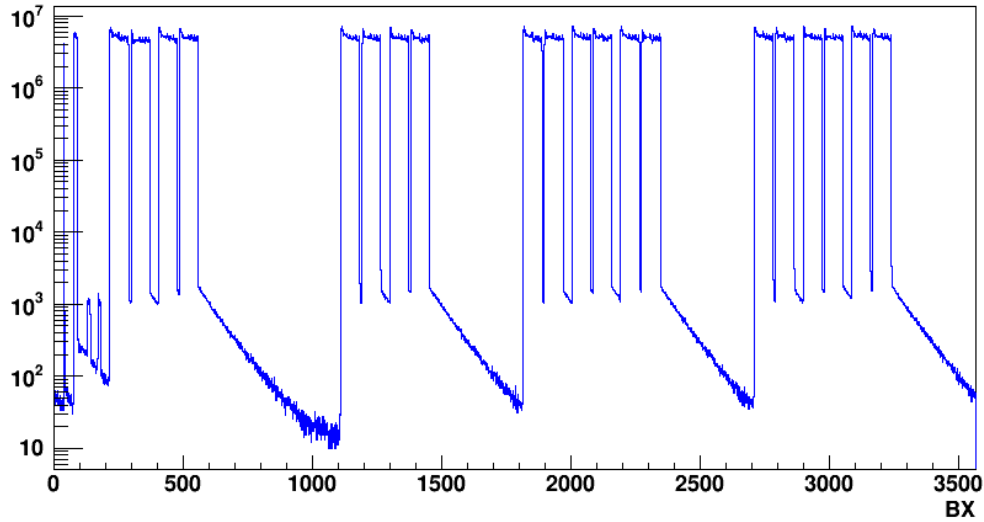


Figure 5.1: 3-fold coincidence count for all channels as a function of bunch crossing, Fill 4444 (2015).

telescope, at the end of a nibble period, receives only around 300 coincidences out of 4096 orbits as shown in figure 5.1. The coincidence count is the boolean count of whether there was some coincidence or not. For each telescope, coincidence count (N) is then translated to luminosity value via the zero-counting algorithm in the form of $-\log((4096 - N)/4096)$.

Table 5.1: Time units

| Unit | Value |
|----------------|-------------|
| 1 orbit | 11245 Hz |
| 1 nibble | 4096 orbits |
| 1 lumi section | 64 nibbles |

Contribution from non-colliding bunches

As seen in Figure 5.1, coincidences are also recorded for non-colliding bunches. This contribution could be from the background, secondary interactions, or spill-over from preceding bins.

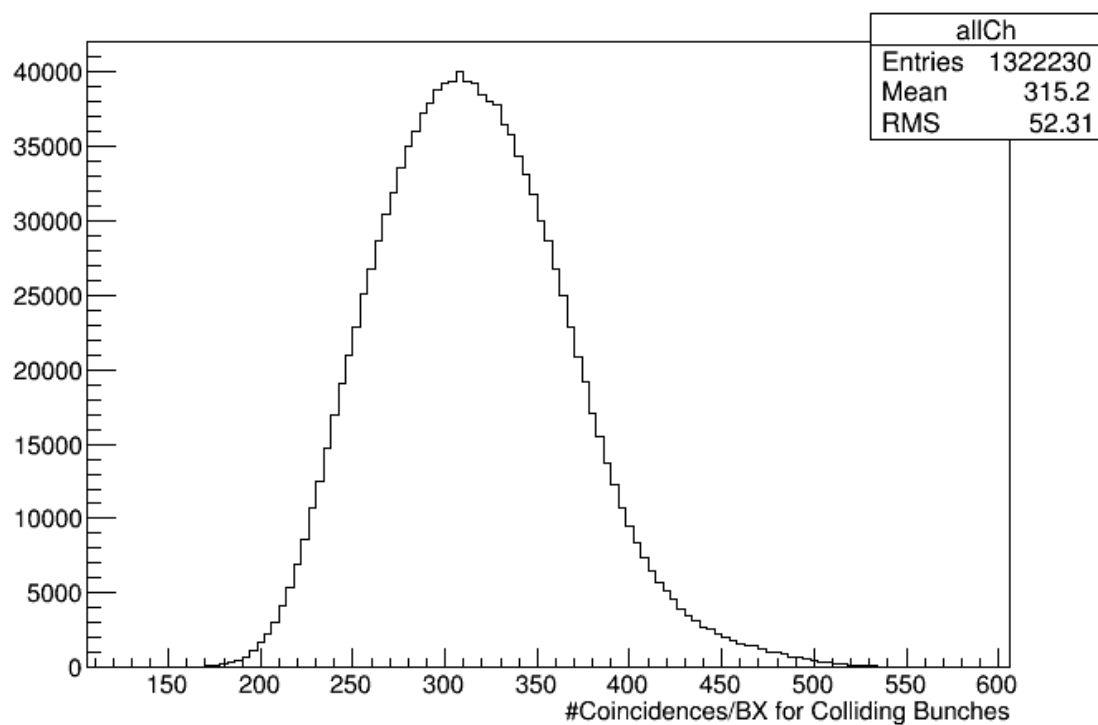


Figure 5.2: Coincidence counts for filled bunches count per nibble, Fill 4444 (2015).

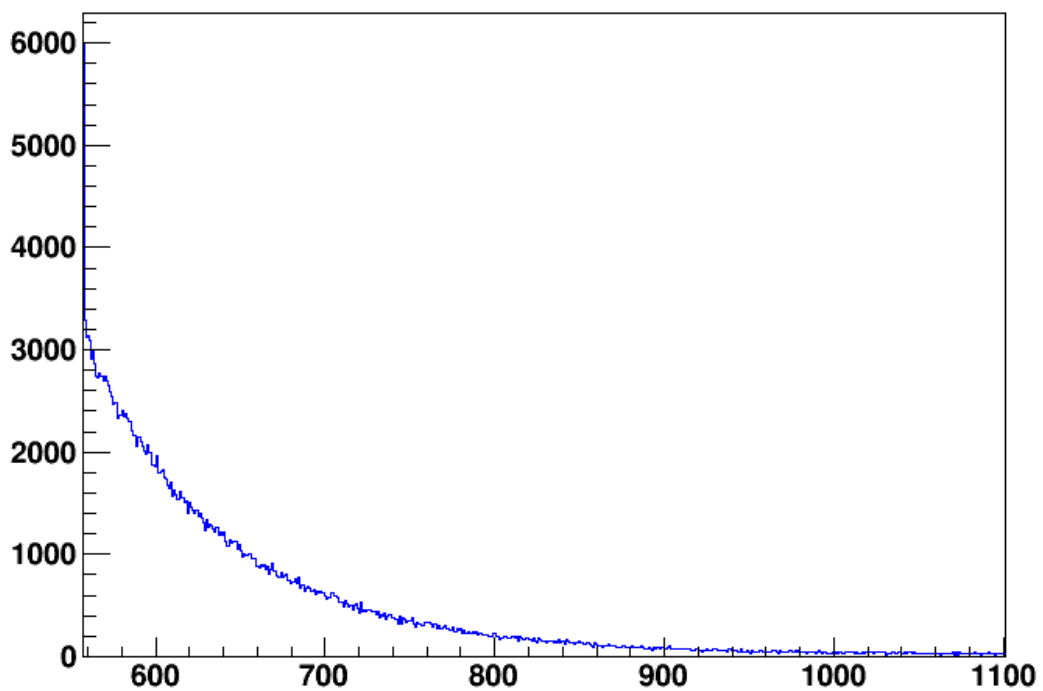


Figure 5.3: Exponential drop in contribution from non-colliding bunches as a function of bunch separation from the last filled bunch.

Figure 5.3 shows the exponential decay in contribution as a function of separation between bunches. The first non-colliding bunch is at 0.1% of the preceding colliding bunch. Except for the first non-colliding BX immediately after filled BX, exponential drop (defined by tau of ≈ 90 BX) can be seen for all gaps. As such, contributions from non-colliding bunches is extremely low.

5.3 Slink Tracks

As described in section 3.4, slink is designed to save only some of the hit information based on some predefined trigger setup. Fig. 5.4 shows the number of tracks per bunch crossing. The tall towers represent the colliding bunches and the rest are the non-filled bunches. Contribution from non-filled BX is very low.

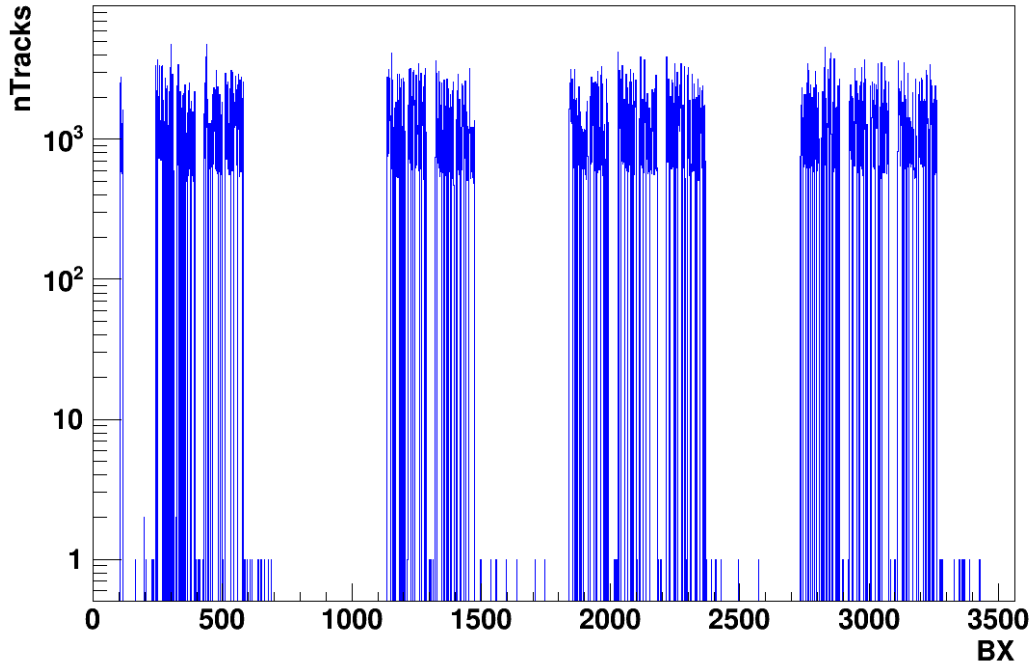


Figure 5.4: nTracks (log) per BX, Fill 4444 (2015) at random trigger.

Given a set of hits on a set of planes, the tracking algorithm is used as described in 5.1 to make tracks which can then be used to parametrize the measurement dataset.

For each track, reconstruction of slopes and residuals in x and y-direction, and the beam spot position are described below.

Track Slopes

The best fit line drawn for a set of hits on 3 planes have slopes that are defined by the geometry of the PLT. Since the telescopes are placed at some angle to the interaction point in the y-direction of the CMS coordinate system, the mean y-slope centers around the PLT global position. At the same time, x-slope is centered around 0 because there is no preferred direction for a track to go in the x direction. Figure 5.5 shows the x and y slopes for a sample of tracks. Slope-y is centered around 0.027 and slope-x is centered around 0.0 as expected.

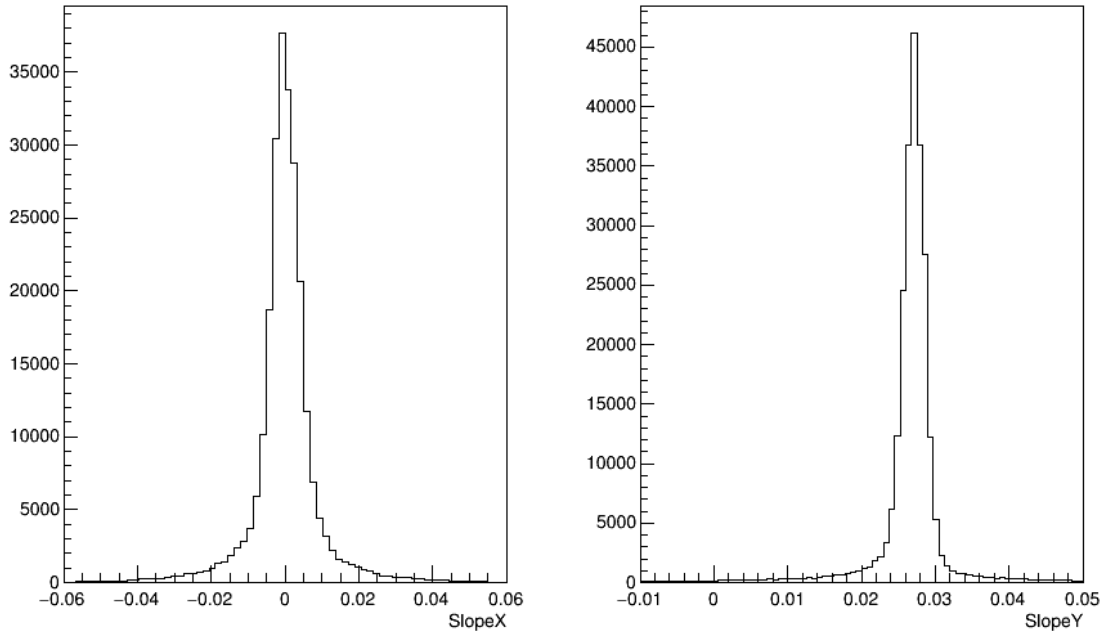


Figure 5.5: Reconstruction of slope-x and slope-y.

Track Beamspot

Beam spot is defined as the position of the track in the x-y plane at the interaction point i.e. at $z=0$ in CMS coordinate system. Figure 5.6 shows the beam spot(cm) seen by the telescopes in both sides of the interaction point from Fill 4444, 2015. The inner blue ring is an ellipse drawn such that major and minor axis represent 3σ of x and y mean separately. The center of the ellipse is positioned at (\bar{x}, \bar{y}) . Most of the tracks seem to be coming from within 2.25 cm of the IP, the beampipe size. The "arms" arise due to the acceptance region of individual telescopes, which is not quite symmetric due to the absence of two telescopes on one side.

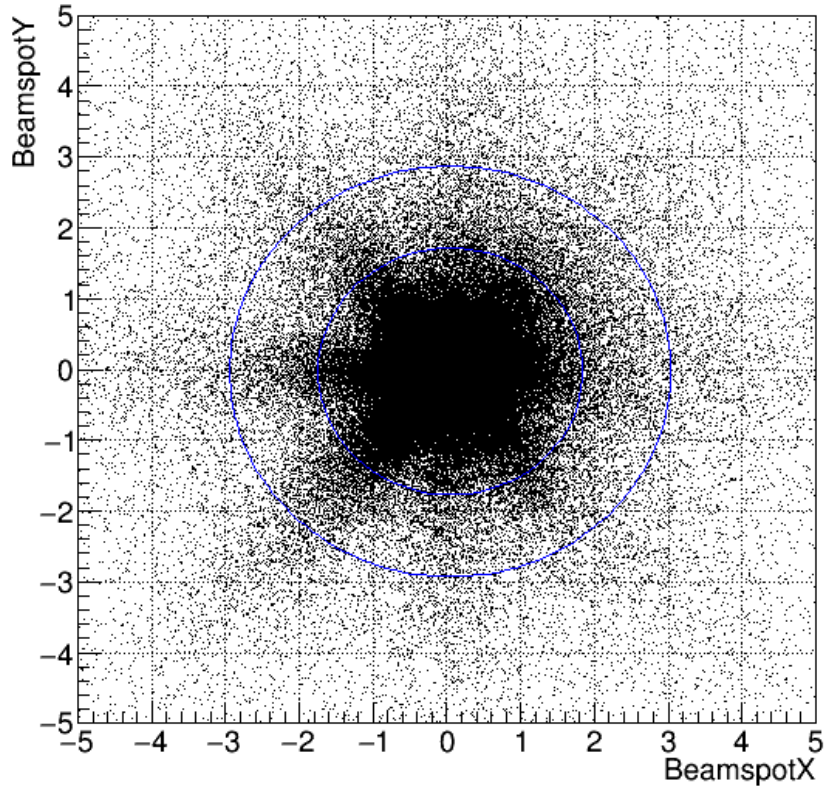


Figure 5.6: Reconstruction of beam spot at $Z=0$ plane. Ellipses drawn at 3 sigma and 5 sigma away from the mean of X, Y.

Track Residuals

Residuals from each track in x and y directions are just the absolute distance between the best of fit line and the position of hits in each plane. Fig. 5.7 shows the x and y residuals for a sample of tracks with a landau-like shape with long tails. The high peak near 0 means that most of the tracks have small residual i.e. the hits of tracks and their best fit line are not very far off. This makes sense because the charged particles have very little time to shift directions in between planes. The discreteness in pixel size, however, introduces some smearing into the residuals. The number of tracks with larger than 3mm residual is extremely low as shown in figure 5.7.

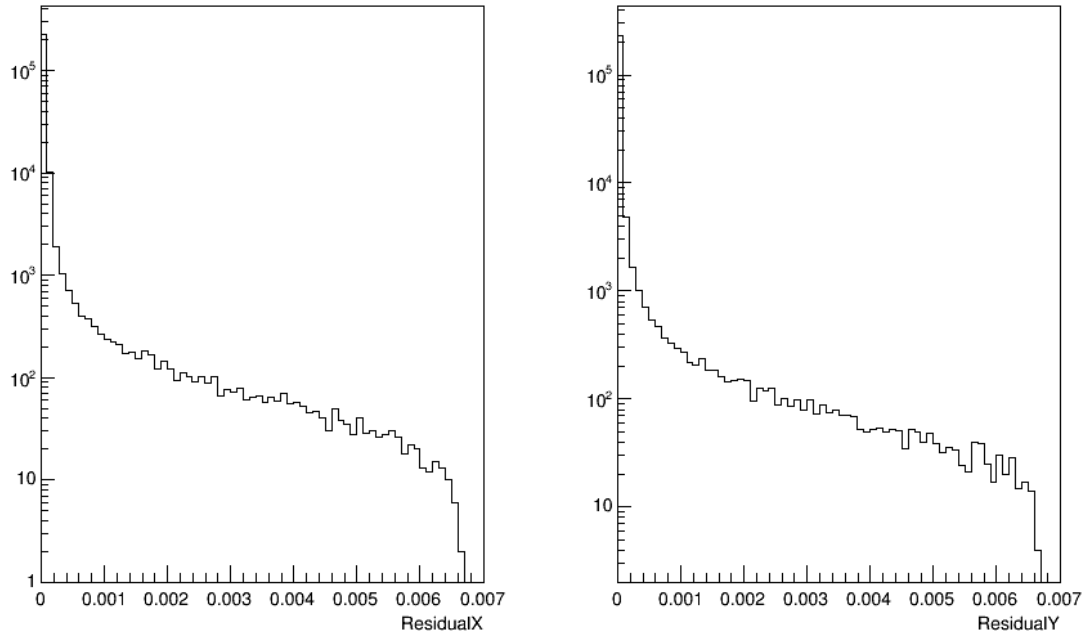


Figure 5.7: Track residuals in x, y direction for a sample run.

Chapter 6

Determination of the Luminosity Correction

6.1 Introduction

The goal of the luminosity measurement experiment is to find the true measure of proton-proton collisions. The LHC sends billions of protons on a head-head collision in a collection of protons called bunches, among which only some protons collide at a given time to produce secondary particles. PLT, located at about 171 cm away from the interaction point and at rapidity, η , of ~ 4 , inclusively measures the charged particles.

Within each filled bunch, the profile of the transverse density of protons is expected to be gaussian. Some protons, however, leak into neighboring bunches as seen in Figure 5.1. Furthermore, protons can collide with elements within the beam pipe to produce spurious tracks. Some protons leave the ideal orbit and interact with rest gas atoms as the vacuum is not perfect, which causes secondary particle production resulting in extra tracks. Fig. 6.1 shows a schematic of tracks from several sources that can be distinguished via the track parameters—slopes, residuals. Generally, the tracks that PLT detects can be categorized as follows:

- 1. Tracks from IP + lumi
- 2. Tracks from IP with scatter + lumi
- 3. Tracks parallel to beam from collision with beam gas and obstructions far away from the IP - extra

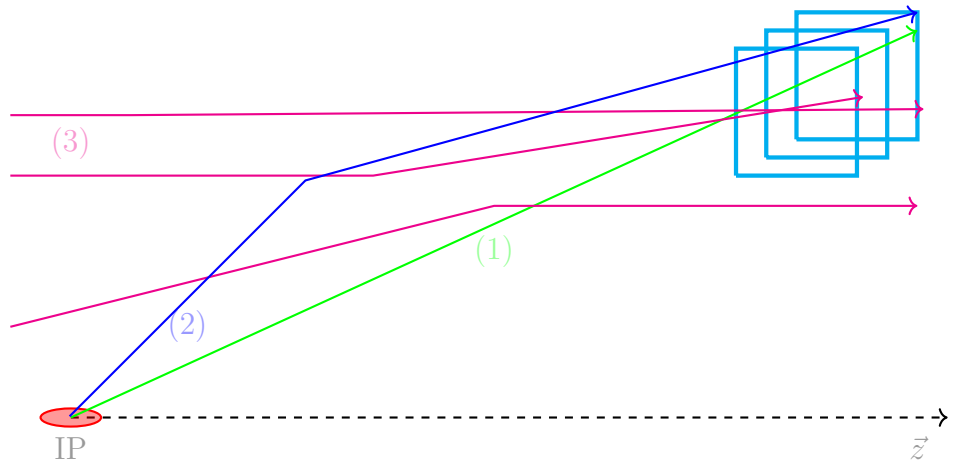


Figure 6.1: Different sources for tracks entering the PLT during proton-proton collisions. IP refers to interaction point and is the origin of genuine tracks responsible for luminosity.

Two different procedures were applied for quantifying the correction term due to accidental tracks for luminosity in 2015 and 2016. Early 2015 data was compromised by the "bug" introduced during the firmware update. Algorithms used to replicate the effect in the luminosity measurement introduced by the bug will be described in section 6.2, firmware issue. Procedures used to find the corrections based on track parameters for 2015 and 2016 are described in section 6.3.2 and section 6.3.3 respectively.

For the 2016 data, vdm scan data was used as a baseline to define track parameters. During vdm scan, 32 bunches are made to collide out of 3564 bunches. This means there is a very small chance of the measured events to have originated from the secondary collision as mentioned earlier. Section 6.3.3 describes the theory behind the maximum likelihood fit method used to parametrize track parameters from the

vdm scan and section 6.4 provides the resulting fit to higher luminosity regime to assign a correction as a function of luminosity itself.

6.2 Firmware Issue

On July 31, 2015, a software bug got introduced while making a firmware update which affected how Fast-OR recognized more than 3 hits on a plane. A hit on a given plane corresponds to a charge deposit above a threshold. This charge is translated into a numerical value by the ADC in the FED. The charge deposits in every other double column are added together. Up to three levels of this signal can be distinguished to arrive at a multiplicity count inside the detector plane. The ADC value range is smaller than the dynamic range of the possible charge deposits of more than 2 hits and hence saturates. Instead of repeating the highest saturation value at high multiplicity the value was set to zero in the FED with this firmware upgrade. Hence, it reported no hit and even if the other two planes also registered at least one hit the FED would not recognize this as triple coincidence. As a result, the coincidence count underestimated by a small fraction as the likelihood for 3 hits or more on a single plane was low. To correct for this effect it was implemented algorithmically. It was decided with a counting of such cases from the ADC values obtained from a transparent buffer.

To understand the effect of firmware issue, one has to know how FED receives signals of hits from each plane sensor. Every sensor is divided into 52 columns which are grouped into 26 double columns. Column (1,2), (3,4), (5,6) and so forth. Fast-OR records the occurrence of hits on a given double column, checks if there were hits on other two planes, and saves the result as 0/1 based on whether there was a triple-coincidence or not. The firmware undercounted the triple coincidences when one or more panels had more than 3 double columns hits for a given time period. To account for this issue, the correction was described with full pixel data. As this data contains all registered hits the expected Fast-OR rate was calculated with events that

had less than 3 hits. This rate can then be compared to accurate counts from the full pixel data to get the correction factor.

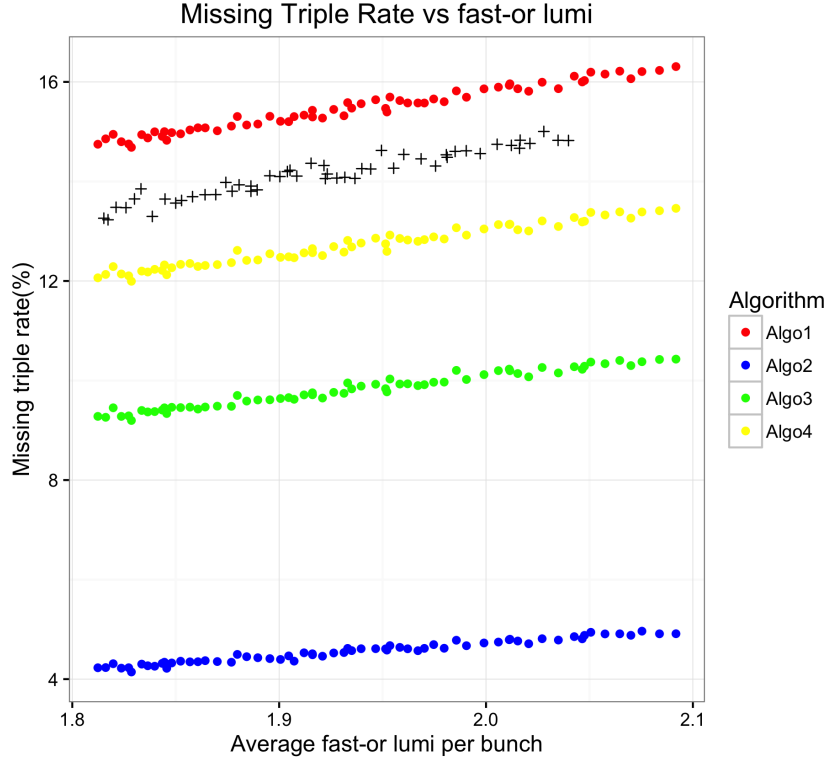


Figure 6.2: Missing Pixel rate from Fill 4444 averaged over 5 minute interval. Missing rate from the transparent buffer is represented by +.

The red points(algo1) simply counts the number of double columns and is, therefore, higher than the rate from the transparent buffer. This overcounting occurs as adjacent double columns are blinded by choice of the trigger on the readout chip. The yellow points(algo4) includes the requirement for adjacent columns on both rows and columns and is, therefore, lower than red and lower than the rate from the transparent buffer. This is expected as FED only checks for adjacency requirement on columns. The green points (algo3) counts the number of double columns with non-adjacent columns and the blue points (algo2) simply counts the number of non-adjacent double columns, both of which undershoot the rate found via the transparent buffer. This simply demonstrates that the trigger based on double columns in the

readout chip does not consistently blind adjacent columns. Therefore, an average between algo1 and algo2 had to be found to match the relative rate of missing triple coincidences. This introduces some arbitrariness in the acceptance of the detector. It is included in the calibration constant σ_{vis} . The rate was eventually chosen to be the one taken from the transparent buffer.

6.3 Accidental Correction

There are pure noise or random track contributions to the Fast-OR counting in the PLT that need to be subtracted before translating the Fast-OR rate into luminosity as described in sec 2.4. Two different methods were used to identify such and count accidental tracks. Section 6.3.2 describes the method used in 2015 where we define accidental tracks as those that fall outside a region in the distribution of track parameters. The relative contribution from the sideband populations is used as a relative correction to the luminosity value. Section 6.3.3 describes an alternative method first applied to 2016 data that uses a maximum likelihood fit to track parameters distribution.

6.3.1 Track Parameters

PLT is positioned so that it accepts tracks that originated at the IP coming at a particular angle. Background tracks are less likely to pass through all three planes of the telescope because of the way plane 0, 1, and 2 are positioned. Still, stray protons could collide with other stray protons to produce secondary particles that pass through all planes of a telescope which can be mistaken for genuine tracks. Sub-particles could also collide with instruments/molecules in the tube to make fake tracks.

The slope-y of all tracks is expected to be a distribution with a mean close to the telescope's slope against IP and slope-x mean is expected to be close to 0. The

goal is to look at the data and see how track parameters change with respect to the parameters from the vdm scan where beams were far separated, and SBIL was close to 0.

Track parameters at VdM

Beam conditions for vdm are different than the regular nominal physics operation, with lower beam intensities and a large separation between few dozens of filled bunches. As such, contribution from the background is expected to be lower, esp since the trigger is only set for colliding bunches. Figure 6.3 shows the number of tracks as a function of beam separation during the "Y1 scan" in 0.5σ steps. Special trigger was employed for vdm scan to collect as many tracks as possible. 32 colliding bunches and 5 con-colliding bunches were triggered for Fill 4954.

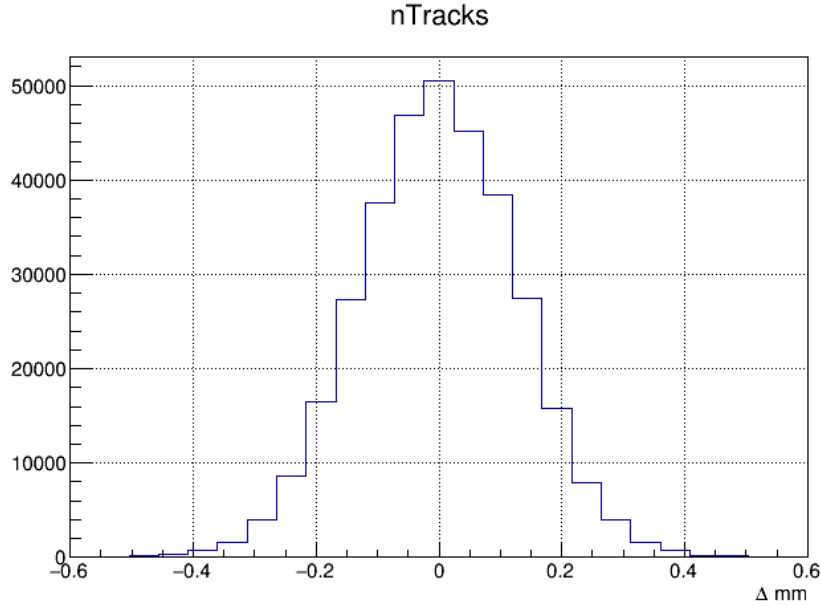


Figure 6.3: Number of tracks vs Beam separation, VdM Fill 4954(2016).

At higher luminosities when the trigger is random and the per instantaneous luminosity is higher, however, non-luminosity contributions as explained in 6.1 are expected to increase. The goal is to find this extra contribution to luminosity measurement as a function of luminosity itself. Probability mass function of track

parameters slope-x and slope-y was constructed using 50566 tracks reconstructed by applying the triple-hit condition for the 0 mm separation of beams during VdM separation scan(Y1). Afterward, deviations from the distributions at higher luminosity was investigated to find out the extra tracks that are seen beyond what is seen at vdm.

6.3.2 5 Sigma Cut Procedure

For the 2015 run period, fill 4444 was chosen as a representative fill where PLT had the least operational issues. Uncertainty to luminosity was assigned by making quality cuts to track parameters. As shown in Figure 6.4, a Gaussian was fitted to slopes and residuals, and tracks falling outside the cut boundaries were investigated.

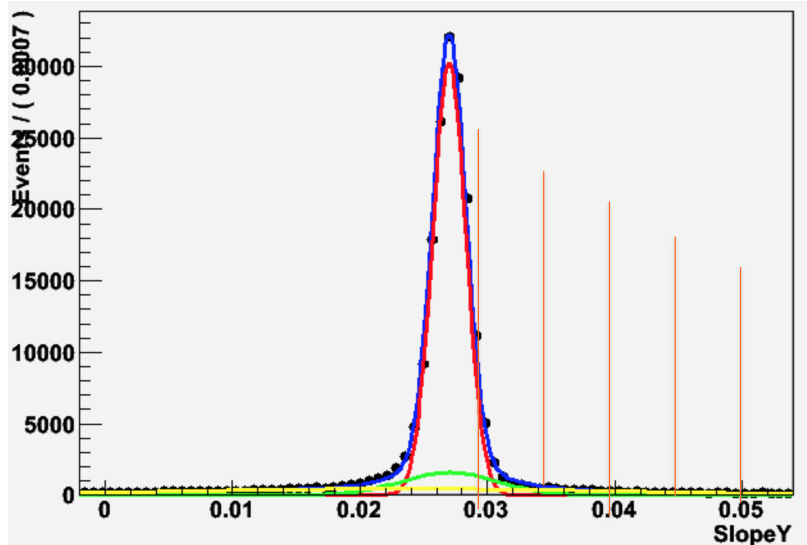


Figure 6.4: Slope-y from Fill 4444 with sigma cut boundaries.

It was found that applying cuts outside 4.5σ to 5σ and 5 to 5.5σ had little impact on the accidental correction. A combined cut of 5σ was applied to both slopes and residuals to define a bad track. Table ?? shows the various cuts applied to slopes and residuals. An uncertainty of 1.5 % is assigned to accidental definition resulting from the change in cut criteria.

Table 6.1: Variation in the measured accidental rate with different sets of cuts in track parameters.

| $ S_x $ cut | $ S_y - S_{PLT} $ cut | R_x cut (cm) | R_y cut (cm) | Measured Accidental Rate |
|-------------|-----------------------|----------------|----------------|--------------------------|
| 0.002 | 0.007 | 0.03 | 0.03 | 11 % |
| 0.03 | 0.0105 | 0.03 | 0.03 | 8 % |
| 0.03 | 0.0105 | 0.02 | 0.02 | 10% |

6.3.3 Maximum Likelihood Fits

Suppose that we have a sample of some n number of independent observations x_1, x_2, \dots, x_n from a theoretical distribution $f(x|\theta)$ where θ is the parameter we would like to find. Let $f(x_1|\theta)$ be the probability of observing x_1 data given θ parameter for function f . Then, the probability of observing x_1, x_2, \dots, x_n data is given by the *likelihood* function

$$L(\theta|x) = f(x_1|\theta)f(x_2|\theta) \cdots f(x_n|\theta) \quad (6.1)$$

Since we have x_1, x_2, \dots, x_n data and we would like to know what θ is, L is maximized by

$$\frac{dL}{d\theta} = 0$$

For distributions of the exponential nature, maximum of the logarithm of L can be found via

$$\frac{d(\ln L)}{d\theta} = 0$$

The solution to $\hat{\theta}$ is the maximum likelihood *estimator* for parameter θ for a given sample. For other samples, $\hat{\theta}$ could be different and thus $\hat{\theta}$ is a probability distribution. The standard deviation on $\hat{\theta}$ gives the size of the error in our estimation for true θ .

Likelihood Fit of slope-x at vdm

The alignment of telescopes is such that there is no preference for slopes to have a particular slope in the x-direction if a track truly originates from the interaction point.

$$VdM_X = \text{Gaussian}_{\text{core}}(\mu_1, \sigma_1) + f_1 * \text{Gaussian}_{\text{outlier}}(\mu_2, \sigma_2) + f_2 * \text{Gaussian}(\mu_3, \sigma_3)$$

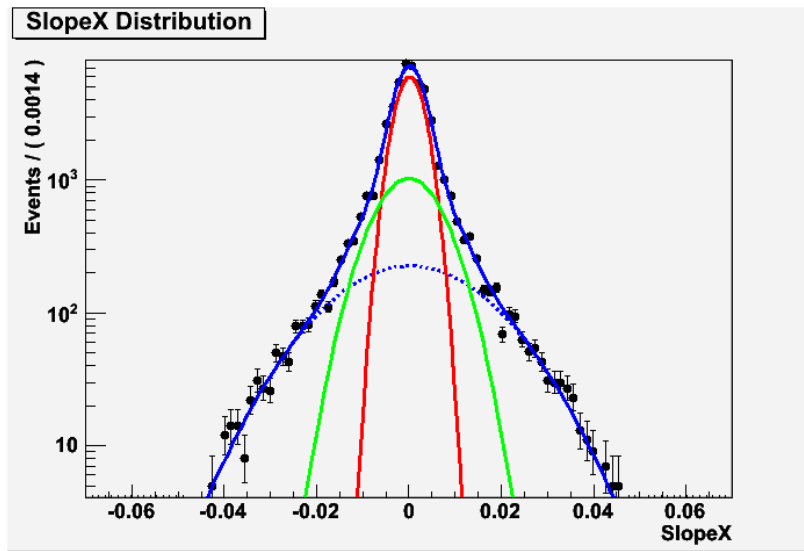


Figure 6.5: SlopeX model using reconstructed tracks from vdm scan at nominal separation.

Fig 6.5 shows the model used for the x -slope of the tracks during VdM Y1 scan Fill 4954. The main signal is dominated by a core Gaussian (red), a broader gaussian (green) and yet another gaussian (dashed blue) that spans the range of x -slope. The mean value for all the pdfs is close to zero, which is due to the fact that there is no reason for a track to have any preference in the $x - y$ plane.

Likelihood Fit of slope-y at vdm

The middle plane of each telescope is placed 0.102 cm higher(lower) than first(third) plane. Since the length of telescope is 7.5 cm, the y -slope of the telescope itself is around 0.027 which is what y -slopes of tracks is expected to be on average.

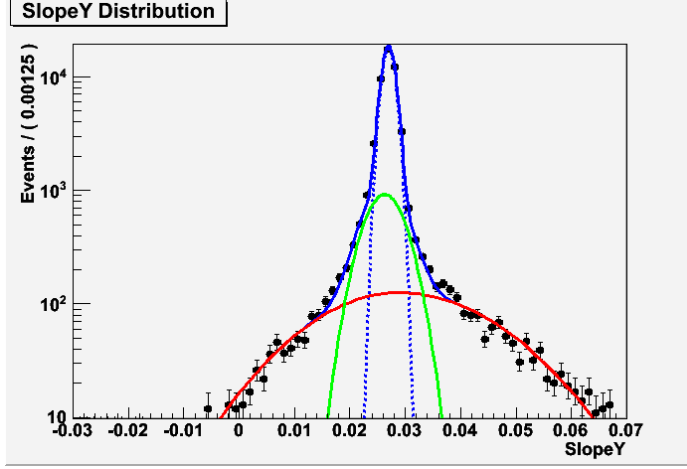


Figure 6.6: SlopeY model using reconstructed tracks from vdm scan at nominal separation.

Fig 6.6 shows the 3 gaussian fit to the slope- y data from VdM Fill Y1 scan. The main signal is dominated by the core gaussian centered at around 0.027, another gaussian, and one bifurcated gaussian with large σ_1 and σ_2 .

$$VdM_Y = \text{Gaussian}_{\text{core}}(\mu_1, \sigma_1) + f_1 * \text{Gaussian}_{\text{outlier}}(\mu_2, \sigma_2) + f_2 * \text{BiGaussian}(\mu_3, \sigma_{31}, \sigma_{32})$$

Combined Fit

A combined model is constructed using the parameters fixed for both slope- x and slope- y with an extra pdf on top of vdm- x and vdm- y models. The extra contribution to the pdf is allowed to float with a common fraction f for both slopes. Figure 6.7 shows the combined fit to one sample data from a regular fill. Both slope- x and

slope- y have a predefined shape of the signal taken from the individual fits to slope- x and slope- y .

$$Combined_Fit = (\text{Vdm_}X + f * \text{Extra_}x) \times (\text{Vdm_}Y + f * \text{Extra_}y)$$

6.3.4 Fit Validation

For each individual fit to slopes, different distributions were tested, including gaussian, polynomials, and double Gaussians. For slope- x , for instance, a double gaussian eventually converged back to a gaussian.

As mentioned earlier, there were 50566 reconstructed tracks from the vdm scan. Some of these tracks, however, came from the non-colliding bunches (5 out of 37 triggered bunches were colliding bunches). The Same fit was done for tracks from colliding and non-colliding bunches separately and it was found that there was not much difference in the fit parameters with the changes.

6.4 Results

The combined model is then fitted to reconstructed tracks from regular fills at higher luminosities. A bifurcated gaussian is used as an extra pdf for slope- y , and a regular gaussian was used as an extra pdf on top of the slope- x model. Figure 6.8 shows the increase in the area under the magenta curve as a function of SBIL. The blue line, $2.2\% + \text{SBIL} * 1.4\%$, is from correction to 2015 data where 5σ cut was applied to slopes and residuals. The black dots which increase with a slope of 0.82 as a function of SBIL, is from 2016 data where likelihood fit method was applied. The fitted line to the black dots goes all the way back to 0, which is the vdm scan with very low value for SBIL. The dotted lines around the black dots represent the uncertainty in the frac3.

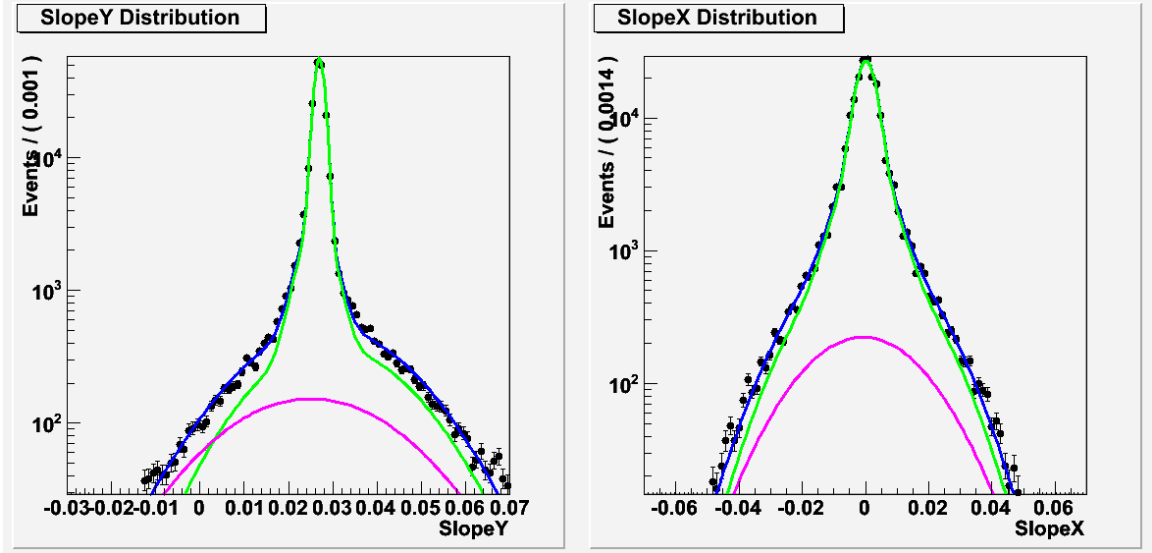


Figure 6.7: Combined Fit to the Model.

6.4.1 Toy Monte Carlo Simulation

A monte-carlo toy simulation was performed to understand the relationship between the accidental cut applied for 2016 data and the fraction of the magenta curve from the likelihood fit. For a sample Fill, 100,000 tracks were generated with parameters from the combined model and the fraction of magenta was fixed to some value. A single gaussian was fitted to slope- x and slope- y separately, and the sigma and mean was extracted. Afterward, the number of tracks falling outside the 5σ cut on slope- x and slope- y was calculated multiple times for a given fraction3. The result is shown in figure 6.9 and it shows a linear relationship between the area under the magenta curve and the 5 sigma cut. The slope from the fit is 0.82, and the intercept is 7.63. Slope less than 1 implies that the area under magenta curve increases faster than the area outside the 5 sigma cut.

It should be noted that the 5 sigma cut applied for 2015 data was on both the slopes and residuals. Maximum likelihood fit was done for the relevant independent variables, the slopes, and residuals are simply taken as a measure of track quality. A correction was then applied to the 5 sigma cut procedure that was applied to 2015 data.

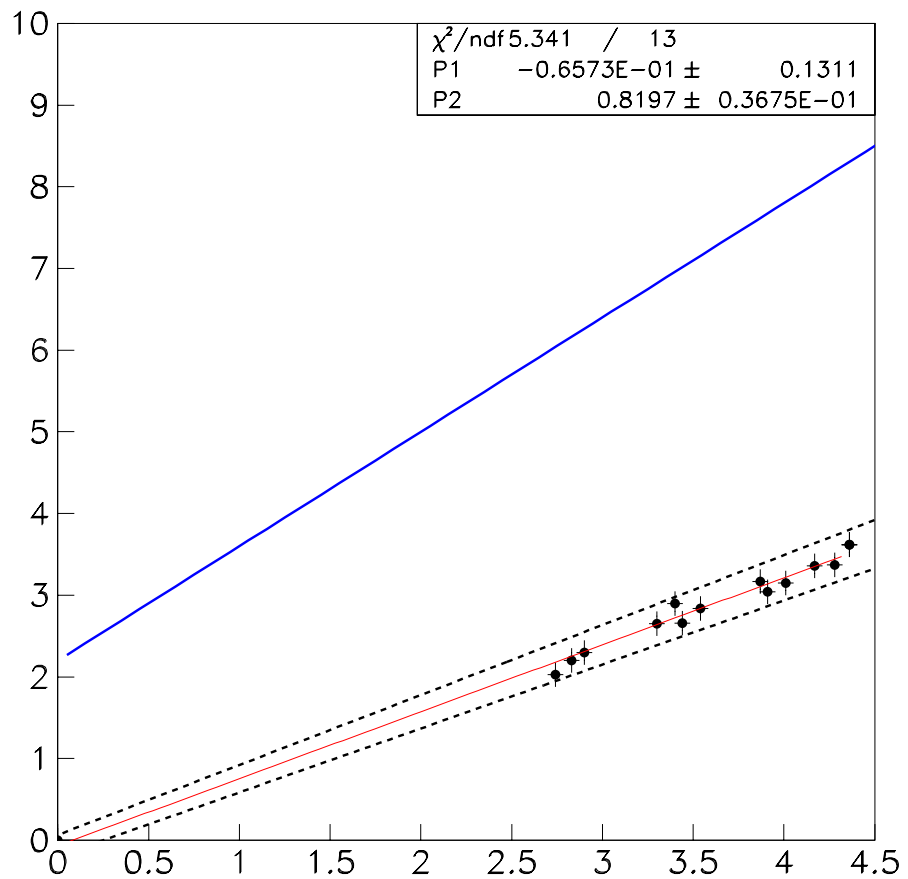


Figure 6.8: Coorection as a function of Single Bunch Instantaneous Luminosity (SBIL). The dashed line correspond to the error bars in fraction of non-lumi contribution.

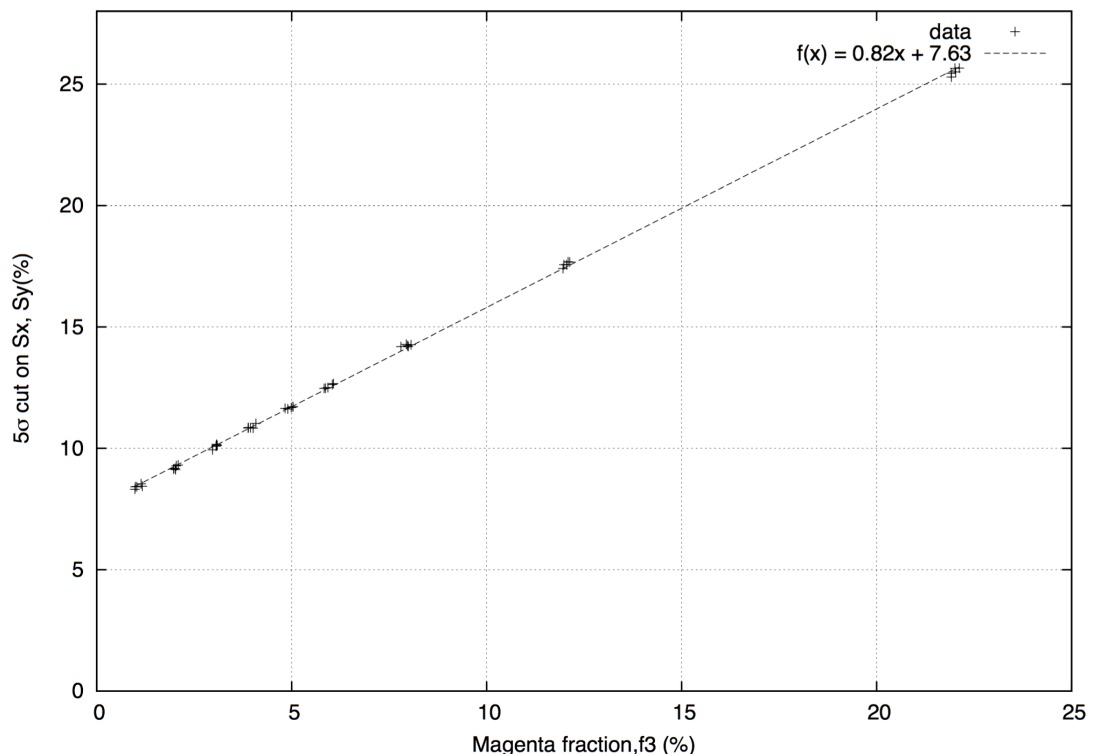


Figure 6.9: Extrapolation of fit model to high accidental fractions vs the counting of the track in tails (outside 5σ) variable distributions.

6.5 Conclusion

I built data pipelines for real-time data visualization and monitoring, wrote alarm system for anomalies detection by inspecting time-series data. I also wrote codes to make event reconstruction, analysis code to make statistical models for classification and prediction of signal and background events in data sets.

Correction to the luminosity measurement by the Pixel Luminosity Telescope (PLT) for the CMS experiment at the Large Hadron Collider was calculated for 2015 and 2016 run period using data-driven statistical methods. The result from likelihood fits was used to improve the background subtraction from nonluminosity contributions.

Bibliography

- Allkofer, Y. et al. (2008). Design and performance of the silicon sensors for the CMS barrel pixel detector. *Nucl. Instrum. Meth.*, A584:25–41. 28
- Bailey, R. and Collier, P. (2004). Standard filling schemes for the various LHC operation modes. *LHC Project Note 323*. x, xi, 8, 17, 18
- Barbero, M. (2003). *Development of a radiation-hard pixel read out chip with trigger capability*. PhD thesis, Basel U., Basel. <https://cds.cern.ch/record/467141>. 27, 28
- Bartz, E. (2005). The $0.25\mu\text{m}$ token bit manager chip for the CMS pixel readout. In *11th Workshop on Electronics for LHC and Future Experiments*. CERN. CERN-2005-011. 27
- Chatrchyan, S. et al. (2014). Description and performance of track and primary-vertex reconstruction with the CMS tracker. *JINST*, 9:P10009. 24
- CMS Collaboration (2016). CMS luminosity public results. <https://twiki.cern.ch/twiki/bin/view/CMSPublic/LumiPublicResults>. xi, 22
- Collaboration, C. (2008). The CMS experiment at the CERN LHC. *JINST*, 3:S08004. 21, 24
- Dabrowski, A. (2014). Upgrade of the CMS instrumentation for luminosity and machine induced background measurements. Technical Report CMS-CR-2014-362, CERN, Geneva. 25
- Englert, F. and Brout, R. (1964). Broken symmetry and the mass of gauge vector mesons. *Phys. Rev. Lett.*, 13:321–323. 4

- Foerster, M. M. (2015). The cms pixel luminosity telescope interface. xii, 25
- Gabathuler, K. (2005). Psi46 pixel chip - external specification. <http://cmspixel.phys.ethz.ch/docs/psi46-readout-chip/psi46v2.pdf>. 27
- Glashow, S. L. (1961). Partial symmetries of weak interactions. *Nucl.Phys.*, 22:579–588. 3
- Hall-Wilton, R., Loos, R., Ryjov, V., Pernicka, M., Schmied, S., Steninger, H., Halyo, V., Harrop, B., Hunt, A., Marlow, D., Sands, B., Stickland, D., Atramentov, O., Bartz, E., Doroshenko, J., Gershtein, Y., Hits, D., Schnetzer, S., Stone, R., Butler, P. H., Lansley, S., Rodrigues, N., Bugg, W., Hollingsworth, M., Spanier, S., and Johns, W. (2009). Results from a Beam Test of a Prototype PLT Diamond Pixel Telescope. Technical Report CMS-NOTE-2009-022. 1, CERN, Geneva. xii, 25
- Herr, W. and Muratori, B. (2003). Concept of luminosity. *proceedings of CERN Accelerator School*. 8
- Higgs, P. W. (1964). Broken symmetries and the masses of gauge bosons. *Phys. Rev. Lett.*, 13:508–509. 4
- Kästli, H. C., Barbero, M., Erdmann, W., Hormann, C., Horisberger, R., Kotlinski, D., and Meier, B. (2006). Design and performance of the CMS pixel detector readout chip. *Nucl. Instrum. Meth.*, A565:188–194. 27
- Kornmayer, A. (2015). The CMS pixel luminosity telescope. *Nucl. Instrum. Meth. A*. 25
- Lujan, P., Riley, G., Rose, K., Spanier, S., and Thapa, K. (2016). PLT luminosity measurement, corrections, and systematic uncertainty for the 2015 run. CMS Analysis Note CMS-AN-2016/002, BRIL PLT. 12, 32
- Pernicka, M., Kotlinski, D., Johns, W., Steininger, H., and Schmid, H. (2007). The CMS Pixel FED. 28

Rossi, L. (2003). Pixel detectors hybridisation. *Nuclear Instruments and Methods in Physics Research Section A: Accelerators, Spectrometers, Detectors and Associated Equipment*, 501(1):239 – 244. Proceedings of the 10th International Workshop on Vertex Detectors. xi, 24

Sakuma, T. (2016). 3d sketchup images of the cms detector (120918). CMS Document 11514-v3. xi, 23

Salam, A. (1968). Weak and electromagnetic interactions. *Conf.Proc.*, C680519:367–377. 3, 4

symmetrymagazine.org (2016). The skinny on the lhc’s heavy ions. [Online; accessed 15-August-2016]. xi, 16

TTCci User Guide (2007). <http://cmsdoc.cern.ch/cms/TRIDAS/ttc/modules/ttcci/>. Accessed: 09-26-2016. 29

User:MissMJ, N. et al. (2014). Standard model of elementary particles. http://commons.wikimedia.org/wiki/File:Standard_Model_of_Elementary_Particles_modified_version.svg. xi, 4

Van Der Meer, S. (1968). Calibration of the effective beam height in the ISR. Technical Report CERN-ISR-PO-68-31. ISR-PO-68-31, CERN, Geneva. 10, 32

Weinberg, S. (1967). A model of leptons. *Phys. Rev. Lett.*, 19:1264–1266. 3, 4

White, S. M., Burkhardt, H., and Puzo, P. (2010). *Determination of the Absolute Luminosity at the LHC*. PhD thesis, Orsay, Universit Paris-Sud 11, Orsay. Presented on 11 Oct 2010. 11

Appendix

A

Pixel Luminosity Telescope

A.1 PLT Channel Map

Table A.1: PLT Channel Map -Z

| Pixel FED Ch | mFEC | mFEC Ch | Physical |
|-----------------|------|------------|----------|
| 01 | 8 | 1 | -N 5 |
| 02 | 8 | 1 | -N 13 |
| 04 | 8 | 1 | -N 21 |
| 05 | 8 | 1 | -N 29 |
| 07 | 8 | 2 | -F 5 |
| 08 | 8 | 2 | -F 13 |
| 10 | 8 | 2 | -F 21 |
| 11 | 8 | 2 | -F 29 |

Table A.2: PLT Channel Map +Z

| Pixel FED Ch | mFEC | mFEC Ch | Physical |
|-----------------|------|------------|----------|
| 13 | 7 | 1 | +N 5 |
| 14 | 7 | 1 | +N 13 |
| 16 | 7 | 1 | +N 21 |
| 17 | 7 | 1 | +N 29 |
| 19 | 7 | 2 | +F 5 |
| 20 | 7 | 2 | +F 13 |
| 22 | 7 | 2 | +F 21 |
| 23 | 7 | 2 | +F 29 |

A.2 Zero - Counting Algorithm

```
if (topic == plthistT::topicname()){

plthistT* dataptr = inheader->getChannelID(); # pointer to data stream

for every nibble:# 1 nibble = 4096 orbits
```

```
lumiNB = 0.0
for (int ch = 0; ch < n_active_channels; ++ch) {
    chLumi = 0.0
    for (int bx = 0; bx < 3564; ++bx) {
        nCoinc[bx] = dataptr->payload()[bx]
        nZeroes[bx] = (4096 - nCoinc[bx])/(4096)
        chLumi[bx] += -log(nZeroes[bx])* calib_factor
        bxzero[bx] = calib_factor * chLumi[bx]
    }
    lumiNB += sum(chLumi)/n_active_channels
}
```

Vita

Krishna Thapa was born in Baglung, Nepal to the parents Pahal and Kalpana Thapa. He has two younger siblings, Pushpa and Yogendra. He attended Texas A&M University in College Station, TX for his Bachelors in physics. Krishna graduated with masters in Physics from the University of Tennessee in Fall, 2016.